Performance Evaluation of Optically Preamplified M-ary PPM Systems for Free-Space Optical Communications

by

Sanaa Hamid

A Thesis Presented to the Faculty of the

American University of Sharjah

College of Engineering

in Partial Fulfillment of

the Requirements

for the Degree

Master of Science in

Electrical Engineering

Sharjah, United Arab Emirates

June 2013

Acknowledgements

I would like to sincerely thank my respectful advisors, Dr. Mohamed Hassan, Dr. Aly Elrefaie and Dr. Taha Landolsi for their supportive guidance, intelligent supervision, and observant remarks which led to the completion of this thesis. I enjoyed our weekly meetings that strengthened my technical knowledge, research capabilities, and organization skills. It was a great pleasure to work with such great professors.

I express my gratitude towards the Electrical Engineering Department of the American University of Sharjah for providing me with the graduate teaching assistantship. I would also like to thank Dr. Khaled Assaleh, Dr. Hasan Al-Nashash, Dr. Verica Gajic, and my advisors for teaching me during my Master's courses. I appreciate their great efforts in classes that broadened my knowledge and assisted in my research. I would like to show my appreciation to Dr. Naser Qaddoumi, Dr. Maher Bakri-Kassem, Dr. Hasan Al-Nashash, Mr. Ibrahim Abu Seif, Mr. Wasel El Tahir, and Mr. Narayanan Madathumpadical for the enjoyable teaching experience I gained while assisting them.

I am thankful to all my friends, whom if I start to mention, the list will never end. I thank my friends back in Sudan for their encouragement to start my Master's studies and for their periodic checks into my progress. I thank my friends at AUS who made my experience in this country wonderful.

I am sincerely grateful to my father and mother whom ultimately supported me, guided me throughout all the stages of my life, and most importantly taught me how to be independent, confident, and honest.

To my parents, brothers and sisters.. . .

Abstract

M-ary pulse position modulation (M-ary PPM) has been widely considered as an attractive solution for increasing the bit rates in free-space optical (FSO) communications. Besides increasing the bit rate, M-ary PPM increases the power efficiency of FSO systems. Hence, better performance can be achieved at lower E_b/N_0 values when compared to on-off keying (OOK). M-ary PPM systems can be implemented using optically preamplified, direct detection receivers. Furthermore, M-ary PPM can be combined with polarization division multiplexed-quadrature phase shift keying (PDM-QPSK) or with PDM-binary phase shift keying (PDM-BPSK) and then detected using optically preamplified coherent detection receivers based on phase/polarization diversity techniques.

In this thesis, the performance of optically preamplified, direct detection 16-ary and 64-ary PPM systems in terms of the bit error ratio (BER) is evaluated. Simulation techniques were used to evaluate the BER without the need to assume that the noise at the decision sample is Gaussian. The combined effects of the dual polarized amplifier noise, the Fabry-Pérot optical filter, the extinction ratio (ER) of the optical transmitter, and the electrical filter at the receiver are all considered in the evaluation. The bandwidths of the optical and electrical filters at the receiver were optimized to obtain the best performance. In addition, the penalties due to frequency drift and timing jitter are also calculated. Simulation results provide the E_b/N_0 values at a target BER of 10^{-3} due to the availability of FEC codes that can reduce the input BER down to 10^{-12}. Four systems with different pulse shapes under an ER value of 20 dB were considered. In each case, the optimum filters were used. For 16-ary PPM systems, those values are 8 dB for the rectangular pulse and 8.2 dB for the $\sin^2$ pulse, while for 64-ary PPM systems, those values are 8.35 dB for the rectangular pulse and 9.6 dB for the $\sin^2$ pulse, respectively. This result indicates that under an ER value of 20

dB, 16-ary PPM systems require smaller values of E_b/N_0 when compared to 64-ary PPM systems to achieve the same BER. In addition, 16-ary PPM systems have better bandwidth efficiency compared to 64-ary PPM systems.

Also, the E_b/N_0 performance of optically preamplified coherent M-ary PPM combined with PDM-BPSK and with PDM-QPSK systems is evaluated. The performance penalties due to finite ER values are also evaluated. For PDM-QPSK 8-ary PPM systems, the penalty at 20 dB ER is 0.5 dB and for PDM-QPSK 16-ary PPM systems is 1.5 dB, while for PDM-BPSK 8-ary and 16-ary PPM systems, the penalty is 1 dB and 2.6 dB, respectively. For 64-ary PPM systems combined with PDM-QPSK or PDM-BPSK, the penalty at 20 dB ER is much larger than 7 dB, which indicates the impracticality of these systems.

Search Terms— Optically Preamplified Receivers, Direct Detection, Coherent Detection, M-ary Pulse Position Modulation (PPM), Fabry Pérot Filters, Extinction Ratio, Polarization Division Multiplexed (PDM), Binary Phase Shift Keying (BPSK), Quadrature Phase Shift Keying (QPSK).

Table of Contents

List of Figures

List of Tables

List of Abbreviations

APD	-	Avalanche Photo Detector
ASE	-	Amplified Spontaneous Emission
BER	-	Bit Error Ratio
BPSK	-	Binary Phase Shift Keying
DLI	-	Delay Line Interferometer
EDFA	-	Erbium-Doped Fiber Amplifier
FEC	-	Forward Error Correction
FP	-	Fabry-Pérot
FSO	-	Free-Space Optical
FWHM	-	Full Width Half Maximum
GEO	-	Geostationary Earth Orbit
HAP	-	High Altitude Platform
IM-DD	-	Intensity Modulation-Direct Detection
LED	-	Light Emitting Diode
LEO	-	Low Earth Orbit
NRZ	-	Non-Return-to-Zero
OOK	-	On-Off Keying
PBS	-	Polarization Beam Splitter
PDM	-	Polarization Division Multiplexed
POLSK	-	Polarization Shift Keying

PPB	-	Photons Per Bit
PPM	-	Pulse Position Modulation
PQ-PPM	-	PDM-QPSK PPM
QPSK	-	Quadrature Phase Shift Keying
RZ	-	Return-to-Zero
SNR	-	Signal-to-Noise Ratio
SWaP	-	Size, Weight, and Power
UAV	-	Unmanned Aerial Vehicles

Chapter 1

Introduction

1.1 Free-Space Optical (FSO) Communication Systems

FSO communication systems utilize modulated laser beams propagating between two optical terminals to form line-of-sight (LOS) free-space links. Unlike radio frequency (RF) communication systems, FSO communication systems enjoy an abundance of bandwidth without the need for spectrum licensing. The transmitted optical power in FSO systems can be focused into very narrow laser beams. This ability eliminates interference and increases the achievable bit rate-distance products (e.g., links with bit rates in the range of Gbits/s and distances in the range of tens of thousands kilometers). However, using very narrow laser beams requires accurate acquisition pointing and tracking (APT) control systems to ensure continuous alignment of the optical terminals. Optical terminals are usually smaller and lighter than RF terminals. This property, in addition to the ability to transmit at high data rates, gives an advantage to FSO communication systems over RF systems in many applications. However, when mobility is considered, RF communication systems are superior to FSO communication systems although the former is typically characterized by their low bit rate-distance products [1].

Figure 1.1 illustrates some examples of FSO links and their corresponding distances. FSO optical terminals can be used to form various types of networks between buildings in what is known as terrestrial links. Terrestrial links are useful when high data rates are needed, especially when it is difficult to construct fiber-optic links [2]. However,

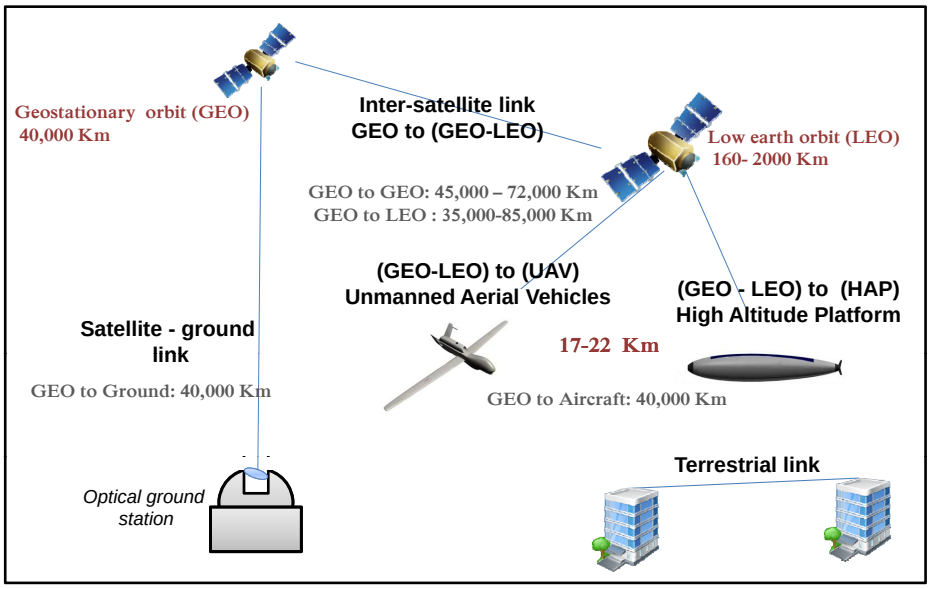

Figure 1.1: Examples of FSO Links and Corresponding Distances.

they are affected by atmospheric conditions. FSO links can also be used to form inter-satellite communication links [3]. These include links between two low earth orbit (LEO) satellites with a distance of 15,000 km, between two geostationary orbit (GEO) satellites with distances between 40,000 and 84,000 km, or between a GEO to a LEO with distances up to 85,000 km [4].

Other examples of FSO systems include satellite to aircraft links. These systems are of recent interest and still encounter many challenges [5]. The major challenge is that the continuous and fast movement of aircrafts imposes strict requirements on APT systems. Examples of these systems include communication with unmanned aerial vehicles (UAV) [6], with airplanes [7], and with high altitude platforms (HAP) [8, 9, 10]. Some of the applications of FSO communication with HAP include constructing optical backhauls [11] and data rely systems [12]. Furthermore, FSO links can be used in satellite to ground base optical station communications [4, 13] and for deep-space and interplanetary communications [14, 15] where the link distance usually extends to millions of kilometers.

It is desired in FSO systems to reduce the size, weight and power (SWaP) requirements of the optical terminals [16]. SWaP can be reduced through increasing the receiver

sensitivity, which is defined as the minimum optical power, or alternatively, the minimum number of photons per bit (PPB) required to achieve a desired bit error ratio (BER) for a given modulation scheme. Higher sensitivity leads to a smaller antenna diameter and thus reduces SWaP.

Several modulation schemes have been considered for FSO communication systems. Non-return-to-zero (NRZ) and return-to-zero (RZ) on-off keying (OOK) modulation schemes have been extensively analyzed for FSO communications [17]. The direct detection-based OOK, also known as intensity modulation with direct detection (IM-DD), has been widely implemented due to the simplicity of the optical receivers. Coherent modulation schemes have also been considered since they offer better performance than OOK systems [18]. Homodyne binary phase shift keying (BPSK) has been examined and implemented for inter-satellite communications at bit rate of 5.65 Gbps as described in [3] and recently demonstrated in [19] at a bit rate of 9.94 Gbps. M-ary pulse position modulation (PPM) has been also studied and evaluated in [20, 21, 22, 23] as a promising modulation scheme capable of offering better sensitivity and higher data rates at reduced power consumption. Recent attempts to achieve higher efficiency than conventional M-ary PPM systems include demonstrations of combined modulation formats such as polarization division multiplexed quadrature phase shift keying (PDM-QPSK) with M-ary PPM using coherent techniques [24].

Many FSO links were successfully implemented and tested [25], where the dominant technology was based on IM-DD and on beacon-assist for tracking. In 1995, the Ground Orbiter Lasercomm Demonstration (GOLD) resulted in a 1 Mbps optical link between a Japanese GEO and the Table Mountain Facility (TMF) in the USA [4]. In 2001, the Geosynchronous Lightweight Technology Experiment (GeoLITE) was launched by Lincoln Laboratory to achieve a duplex 1550 nm downlink between the GEO and the ground [4, 25]. In the same year, the Semiconductor Inter-Satellite Lasercom Experiment (SILEX) was held by the European Space Agency to accomplish a duplex LEO to GEO 50 Mbps link [26]. Later in 2002, the Airborne Laser EXperiment (ALEX) by Lincoln Laboratory was conducted leading to a duplex 1 Gbps GeoLITE air link [4]. In 2005,

the Japanese space agency (JAXA) accomplished LEO to GEO and LEO to ground links and later in 2006, Liaison Optique Laser Aéroportée conducted a 50 Mbps duplex link to SILEX [27]. Finally in 2008, the German company, Tesat-Spacecom, launched a 5.65 Gbps LEO to LEO link using beacon assist and coherent BPSK receivers [4].

1.2 Motivation

Future FSO applications and services are expected to demand higher bit rate-distance products. Current modulation schemes used in FSO communication systems such as NRZ and RZ-OOK set an upper limit on the achieved data rates, especially for inter-satellite links that are characterized by high distances. Therefore, to increase the bit rate at high transmitter-receiver distances while improving the BER performance, more efficient modulation schemes such as M-ary PPM with direct detection and M-ary PPM combined with PDM-QPSK with coherent detection need to be considered. Along with the recent advances in optical technology, error correcting codes, and digital signal processors (DSPs), such optical modulation schemes have become viable alternatives to current modulation schemes.

1.3 Contributions

The main contribution of this thesis is the evaluation of the BER performance of optically preamplified direct detection 16-ary and 64-ary PPM systems. Simulation techniques were used to evaluate the BER without the need for the analysis that assumes that the noise at the decision sample is Gaussian. The combined effects of the dual polarized amplifier noise, the Fabry-Pérot optical filter, the extinction ratio of the optical transmitter, and the electrical filter at the receiver are all considered in the evaluation. Extensive simulations were carried out to optimize the bandwidths of the optical and electrical filters at the receiver. Furthermore, the performance penalties due to frequency drift and deterministic timing jitter at the receiver are calculated.

The performance of optically preamplified NRZ-OOK systems was also evaluated and compared with M-ary PPM systems. Finally, the performance of optically preamplified coherent systems combining M-ary PPM with PDM-QPSK or with PDM-binary phase shift keying (PDM-BPSK) for $M \in [4, 8, 16, 32, 64]$ was evaluated. Also, the penalties due to finite extinction ratio for $M \in [8, 16, 64]$ in PDM-QPSK M-ary and PDM-QPSK M-ary PDM-BPSK were calculated.

1.4 Thesis Organization

The rest of this thesis is organized as follows. In Chapter 2, optical modulation schemes, optical transceiver components, and link budget calculations for FSO systems are explained. Chapter 3 presents a brief evaluation of optically preamplified OOK systems and Chapter 4 addresses a detailed evaluation of optically preamplified M-ary PPM systems. Chapter 5 discusses the combined modulation formats and Chapter 6 concludes the work presented.

Chapter 2

Background

In this chapter, the modulation schemes that can be used for FSO communication systems are explained. The components of FSO communication systems are illustrated and the differences between various receiver configurations, namely, photon-counting receivers, optically preamplified direct detection receivers, and coherent receivers are demonstrated. Finally, the link budget estimation for FSO communication systems is described.

2.1 FSO Modulation Schemes

The selection of the modulation scheme to be used in FSO communication systems depends mainly on the type of detection, the required BER, and the available detection technology. For direct detection receivers, intensity and some differential modulation schemes are more suitable. The most common formats of digital intensity modulations are the on-off keying (OOK) and the M-ary pulse position modulation (M-ary PPM) which are categorized as pulse-based modulations. In differential modulation schemes, such as differential phase shift keying (DPSK), the bits are differentially-encoded and additional optical devices are added to the direct detection receiver to convert the differential phase information into intensity-based signaling.

Coherent receivers are capable of extracting the phase or the polarization information with the aid of a local oscillator and/or additional optical devices such as polarization beam splitters (PBS) and 90° hybrid devices. Non-pulsed modulation schemes such as phase shift keying (PSK) and polarization shift keying (POLSK) are possible. Coherent receivers are also capable of detecting pulse-based modulation schemes.

Capacity and spectral efficiency of classical modulation formats can be increased by combining more than one modulation format through simultaneous modulation of more than one property of light. Combined modulation formats provide higher sensitivities when compared to classical modulation formats as a result of aggregating more bits in each symbol for the same optical power. In the following subsections, the details of the commonly addressed optical modulation formats are explained.

2.1.1 On-Off Keying (OOK)

In OOK, the binary bits are represented by the presence or absence of the light pulse in the corresponding symbol interval [4, 28]. OOK signaling consists of two symbols and can be categorized into non-return-to-zero (NRZ) and return-to-zero (RZ) signaling. In NRZ-OOK, the symbol (s_1) represents a binary "1" and the symbol (s_0) represents a binary "0" where the waveforms of s_1 and s_0 can be represented as:

$$\begin{aligned} s_1(t) &= A\cos\left(2\pi f_0 t\right), \\ s_0(t) &= 0. \end{aligned} \tag{2.1}$$

NRZ-OOK and RZ-OOK modulation schemes are illustrated in Figures 2.1 and 2.2, respectively. In RZ-OOK, s_1 contains an optical pulse that occupies a portion of the symbol interval [29]. The percentage of the full portion relative to the empty portion is known as the duty cycle. For example, the RZ-OOK waveform in Figure 2.2 has a duty cycle of 50%.

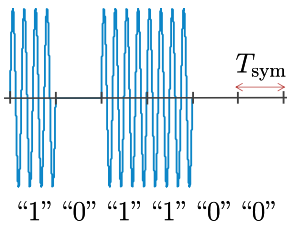

Figure 2.1: NRZ-OOK Modulation Scheme.

RZ-OOK modulation scheme clearly reduces the optical power consumption but increases the bandwidth requirements for the same bit rate. RZ and NRZ-OOK with direct detection have been implemented in most FSO links due to their receiver simplicity [25].

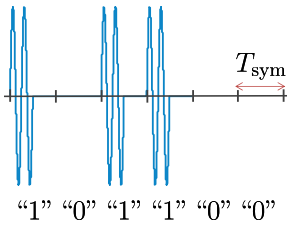

Figure 2.2: RZ-OOK Modulation Scheme.

2.1.2 Differential Phase Shift Keying (DPSK)

Direct detection receivers are usually insensitive to the phase and polarization of the received optical field. However, direct detection of phase- or polarization-based modulation schemes is possible with the aid of additional optical devices [30]. The role of these optical devices is to transform the phase or polarization information into OOK signaling. A differentially encoded phase-based modulation format could be directly detected with the aid of a delay line interferometer (DLI). In DPSK, a binary “1” is encoded as a phase shift of π and a binary “0” as no-phase shift. The role of the DLI is to produce two signals where the second signal is a delayed version of the first one. The two signals are usually connected to a balanced receiver where the output of the first photodiode represents the sum of the two signals and the second represents the difference. When the output of the sum diode is high and the difference is low, “‘0” is decoded since the consecutive symbols have no phase difference. When the output of the sum diode is low and the difference is high, a phase shift of π is detected and a binary “1” is decoded [31]. Figure 2.3 illustrates the structure of the differential receiver.

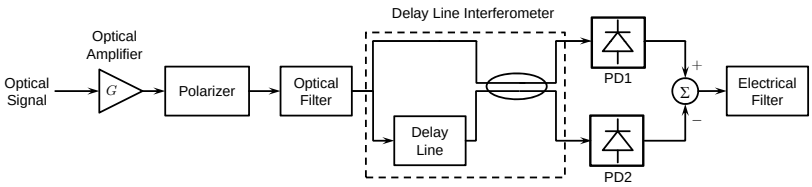

Figure 2.3: DPSK Receiver.

DPSK offers better sensitivities than OOK and provides constant envelop input to the receiver thus reducing the nonlinear effects. The sensitivity of optically preamplified DPSK was recorded in [32]. Results indicated sensitivity of 25 PPB at a BER of 10^{-9}.

2.1.3 Polarization Shift Keying (POLSK)

In POLSK, the data is modulated using the optical field polarization state. For example, in binary POLSK, "1" and "0" are encoded into two orthogonal polarization states. POLSK can be directly detected with the aid of the PBS [33]. In binary POLSK, the PBS at the receiver separates the two orthogonal fields and feeds them into a balanced receiver. POLSK is considered for FSO communications to overcome the effects of atmospheric turbulence [34]. This is because the optical field polarization state is one of the most stable properties of the light while propagating in free-space. POLSK can also be detected coherently to provide higher sensitivities when compared to directly detected POLSK [35, 36].

2.1.4 M-ary Pulse Position Modulation (M-ary PPM)

In M-ary pulse position modulation, each r-bits are translated into a single pulse in one of M distinct positions within the symbol period. The number of bits (r) contained in each PPM symbol is $\log_2 M$. Figure 2.4 illustrates a 16-ary PPM where the slot interval (T_{slot}) is equal to $1/16$ of the symbol interval (T_{sym}). For example, the sequence "0000" is mapped into the 1^{st} PPM slot, the sequence "0010" is mapped into the 3^{rd} PPM slot, and the sequence "1111" is mapped into the 16^{th} PPM slot.

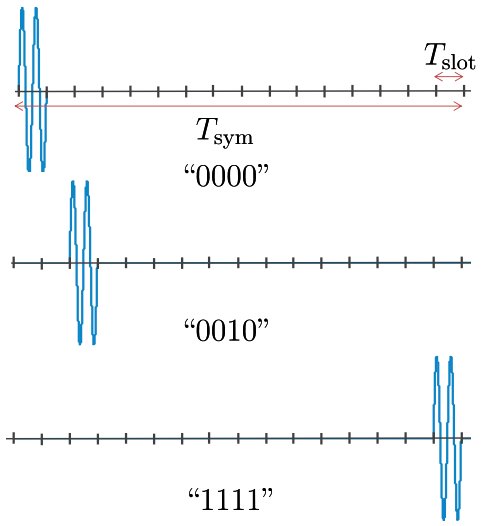

Figure 2.4: 16-ary PPM Modulation Scheme.

M-ary PPM systems are highly desired for FSO communications because they offer higher sensitivities than those provided by OOK systems [20, 21, 22, 37, 38]. M-ary PPM have been demonstrated in [39] with bit rates between 52 Mbps and 311 Mbps, and in [40] with bit rates of 78 Mbps for 256-PPM up to 1244 Mbps for 2-PPM. The study in [41] suggests an implementation for a 12.5 Gbps 16-ary PPM receiver for FSO communications that relies on planner lightwave circuits. M-ary PPM systems have been also considered for fiber links where both optically preamplified direct and coherent detections were studied [42, 43, 44].

2.1.5 Binary Phase Shift Keying (BPSK)

In BPSK, binary data is encoded into two phase shifts (ϕ_1 and ϕ_2) spaced by π. For example, when "0" is represented by $\phi_1 = 0$, "1" is represented by $\phi_2 = \pi$. Figure 2.5 shows the BPSK modulation scheme.

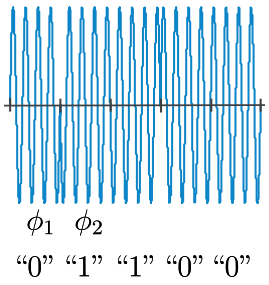

Figure 2.5: BPSK Modulation Scheme.

BPSK has been implemented in inter-satellite links as described in [3, 13, 19]. Those links provide a typical sensitivity of 40 PPB at a data rate of 1 Gbps. Recently, BPSK was demonstrated in [45] with bit rates of 9.94 Gbps and 19.88 Gbps and found to provide sensitivities of 2.1 PPB and 3.9 PPB, respectively.

2.1.6 Quadrature Phase Shift Keying (QPSK)

In QPSK, four phase shifts (ϕ_1, ϕ_2, ϕ_3, and ϕ_4) spaced by $\pi/2$ are used to represent four different symbols ("00", "01", "10", and "11"). Figure 2.6 represents the QPSK modulation scheme. QPSK was considered for FSO communication in [46, 47].

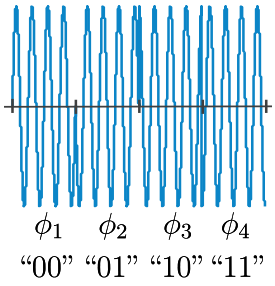

Figure 2.6: QPSK Modulation Scheme.

2.1.7 Combined Modulation Schemes

Combined modulation schemes are achievable by modulating more than one property of light at the same time such as the phase, the polarization, and the pulse position. Examples of combined modulation schemes are polarization division multiplexed quadrature phase shift keying (PDM-QPSK), PDM binary phase shift keying (PDM-BPSK), and PDM-QPSK M-ary PPM.

(a) PDM-BPSK

In PDM-BPSK, two phase shifts ($\phi_1$and ϕ_2) spaced by π in addition to two polarizations states (e.g., x polarization and y polarization) are used to represent four different symbols ("00", "01", "10", and "11"). Figure 2.7 shows the waveform and the lowpass equivalent signal for three symbols of the PDM-BPSK modulation scheme.

(b) PDM-QPSK

In PDM-QPSK, four phase shifts (ϕ_1, ϕ_2, ϕ_3, and ϕ_4) spaced by $\pi/2$ in addition to two polarizations states (e.g., x polarization and y polarization) are used to represent 16 different symbols ("0000", "0001", ..., "1111"). Figure 2.8 shows the waveform and in-phase and quadrature-phase components for three symbols of the PDM-QPSK modulation scheme.

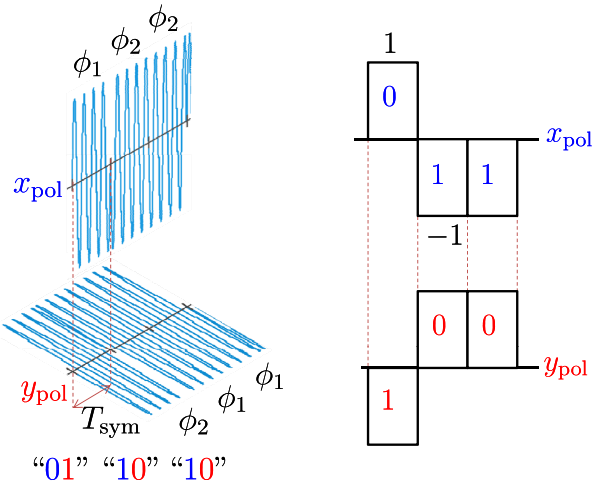

(a) Waveform (b) Lowpass Equivalent

Figure 2.7: PDM-BPSK Modulation Scheme.

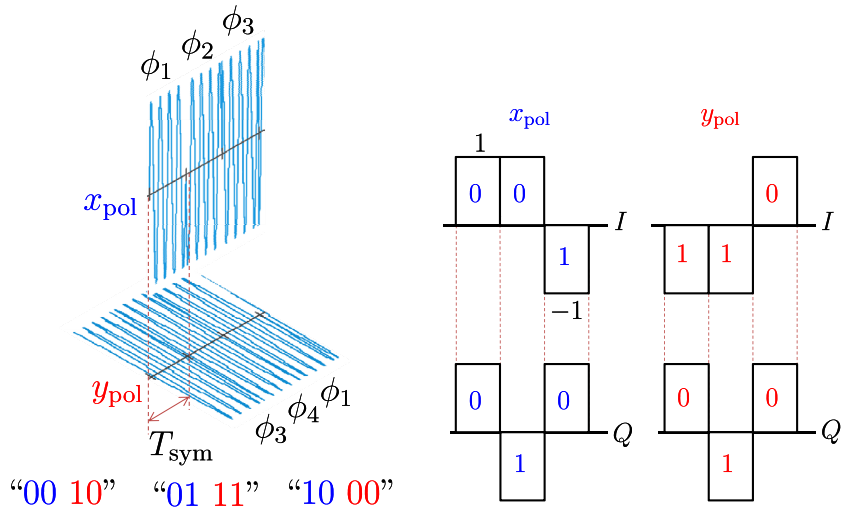

(a) Waveform (b) Lowpass Equivalent

Figure 2.8: PDM-QPSK Modulation Scheme.

(c) PDM-QPSK M-ary PPM

In PDM-QPSK M-ary PPM, the pulse position, the phase, and the polarization of the optical field are used to encode the bits. Figure 2.9 illustrates 16-ary PPM systems which have 2^8 symbols represented by eight bits. The first four bits determine the location of the pulse in one of 2^4=16 slots. The remaining four bits represent the symbols of PDM-QPSK modulation scheme.

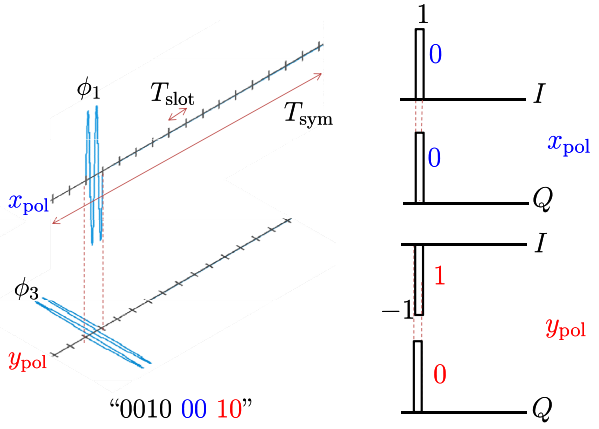

(a) Waveform (b) Lowpass Equivalent

Figure 2.9: PDM-QPSK 16-ary PPM Modulation Scheme.

The implementation of combined modulation schemes in optical communication systems have become realizable through employing digital coherent receivers. In digital coherent receivers, carrier estimation, phase recovery, and demodulation are performed by means of digital signal processing through digital signal processors (DSPs) [48] or field programmable gate arrays (FPGAs) [49]. Thus, the complexities of implementing optical phase locked loops (OPLLs) in coherent receivers are avoided [8]. Another advantage of digital coherent receivers is their flexibility. Several modulation schemes or levels can be implemented on the same digital system by simple modifications to the applied software [50].

DSP based coherent receivers have been considered for dual-mode optical receivers that are capable of detecting IM-DD and BPSK at 6 Gbps or QPSK at 12 Gbps. These systems have been developed and tested for future FSO communication links [51, 52]. The performance of several combined modulation schemes such as polarization-shift-QPSK (PS-QPSK), PDM-QPSK, and PDM-QPSK M-ary PPM was addressed in several studies [53, 54, 55, 56]. PDM-QPSK M-ary PPM was analyzed and demonstrated in [57, 58, 59, 24]. Sensitivities of 3.5 PPB and 2.7 PPB where recorded at a BER of 10^{-3} with bit rates of 2.5 Gbps and 6.23 Gbps using PDM-QPSK 16-ary PPM and PDM-QPSK 4-ary PPM, respectively.

2.2 Components of FSO Communications Systems

Figure 2.10 depicts the general block diagram of an FSO communication system. FSO communication systems are usually bi-directional, thus consisting of optical transceivers that include a transmitter and a receiver in both terminals. For simplicity, Figure 2.10 shows a uni-directional FSO system. In inter-satellite links the only channel impairment is the propagation loss which is explained by the fact that the channel is vacuum which is typically free of any atmospheric effects [60]. The optical transmitter generates the optical carrier and then modulates and amplifies the generated optical signal before being emitted into a free-space link. At the other side, the receiver collects the transmitted optical signal and performs the necessary amplification, filtering, and detection processes. The following subsections describe the components of the optical transmitter and receiver.

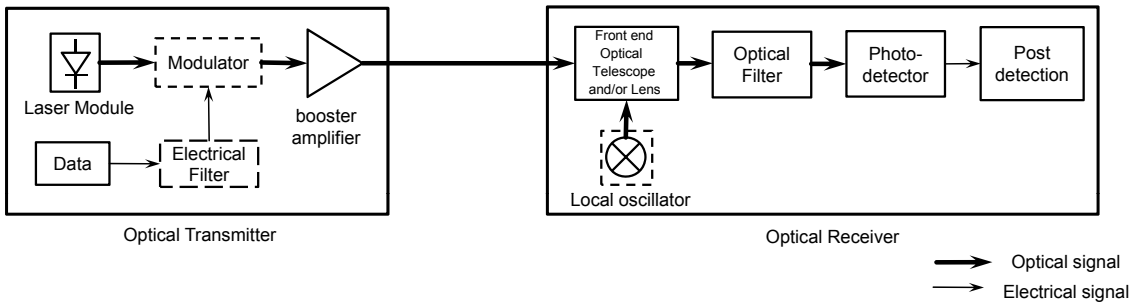

Figure 2.10: A General Block Diagram of FSO Systems.

2.2.1 Optical Transmitters

The optical transmitter consists mainly of a laser source, a modulator, an electrical filter, and a booster amplifier. The laser module generates an optical carrier with a certain desired wavelength. The most widely used wavelength ranges are the (800-900 nm) range and the (1310 or near 1550 nm) range. The first range is preferred for low cost, low data rates, or short distance applications while the second range is preferred for high data rates over long distance applications [2].

The modulation process in the optical transmitters can be performed internally or externally [61]. Internal modulation is achieved by controlling the output of the laser source using the modulating data as a biasing current. The output is then selected to be either on, off, or a controlled amplitude. A simple set of modulation formats can be achieved through direct modulation such as intensity or amplitude modulation. External modulation is achieved through operating the laser device to emit a continuous wave (CW) output. Then, the modulation is achieved externally. A wide set of modulation formats can be performed through external modulation. This includes pulse-based modulations such as OOK and PPM which can be achieved by allowing/blocking the CW into the optical booster amplifier. It also includes phase- and polarization-based modulation formats, where the modulation can be achieved by controlling the electro-optic or acousto-optic effects of the external modulator material on the phase or the polarization of the CW [61, 62]. For high bit rates, external modulators are preferred over internal modulators since they offer faster response and reduced frequency chirp [62]. An optional electrical filter can be used in the optical transmitters to reshape the transmitted optical pulse. Finally, a booster amplifier is used to amplify the optical signal to the desired power level.

2.2.2 Optical Receivers

Optical receivers consist of three main systems: the front end receiving system, the photo-detection system and the the post-detection system [61].

The front end receiving system consists mainly of an optical telescope to collect the transmitted optical signal, and an optical bandpass filter to reduce the excess optical noise. An optical preamplifier might be added to the front end receiving system to increase the sensitivity of optical receivers. The most widely used optical preamplification technology is the Erbium-Doped Fiber Amplifier (EDFA) that operates in the 1.55 μm wavelength window. A drawback of using EDFA amplifiers is the addition of amplified spontaneous emission (ASE) optical noise [62].

One of the most practical optical bandpass filters is the Fabry Pérot filter which consists of a cavity formed by two highly reflective parallel mirrors [29]. The complex base-

band field transfer function of the Fabry Pérot filter can be expressed using the Lorentzian approximation as [17]:

$$B_{FP}(f) = \frac{1}{1 + j2f/\text{FWHM}} \tag{2.2}$$

where FWHM is the full width half maximum or the 3-dB bandwidth.

The photo-detection system converts the optical signals into electrical signals using photodetectors. Photodetectors used in FSO receivers might be a p-intrinsic-n (PIN) device or an avalanche photodetecor (APD) device [2]. PIN photodiodes have an intrinsic (or lightly doped) region between the p-type and the n-type doped semiconductor material. When reverse biased, the internal impedance is significantly large and the diode acts as an open circuit. When photons enter the intrinsic region, electron-hole pairs are produced and an amount of current proportional to the input optical power is generated. The APD consists of a two-layer semiconductor sandwich where the upper layer is n-doped and the lower is heavily p-doped. When reverse biased (i.e., no light received), a dark current is produced due to the thermal generation, and when forward biased, photons reach the p-layer and produce electron-hole pairs. Because the electrical field is strong, electrons can gain enough energy to create secondary electron-hole pairs; a phenomenon known as the avalanche process [2].

APD devices are more sensitive than PIN devices and have internal amplification capabilities that allow the implementation of automatic gain control (AGC) functions in optical receivers. APD devices reduce the need for optical preamplifiers and hence increase the sensitivity without adding ASE noise [4]. PIN devices compared to APD have simpler driving circuitry and lower bias voltages. PIN devices are faster in response and hence more suitable for high data rate systems. In many applications, PIN devices with preamplification are preferred over APD devices [8].

The post-detection system processes the photo-detected electrical signals. It contains the required electrical devices such as electrical amplifiers, electrical filters, as well as demodulation circuity and/or processors.

Optical receivers can be generally divided into three categories: photon-counting

receivers, direct detection receivers, and coherent receivers. Direct detection receivers that utilize optical preamplifiers are known as optically preamplified direct detection receivers. In what follows, each category is illustrated.

(a) Photon-Counting Receivers

Photon-counting receivers are a special type of APD detectors where the internal gain is high enough to enable a few number of photons to generate a binary nature output. In a given time interval, if photons are received "1" is detected, and if no photons are received "0" is detected. Photon-counting receivers are affected mainly by the dark current noise generated when no photons are received [16]. The suitable modulation formats for photon counting receivers are OOK and M-ary PPM [63, 64].

Although photon-counting receivers are efficient, they are not suitable for future high data rate applications [63, 64]. This is due to the limitations induced by the counting process where after each detection event, the photo-detector remains idle for a period of time, known as the reset time, before it can resume counting. However, photon-counting receivers are desired for power-starving links with low data rates such as deep space links. Photon-counting receivers are being considered for the Lunar Laser Communications Demonstration (LLCD) scheduled to be launched in 2013 [65]. The terminals for LLCD employ 64-ary PPM to achieve a 622 Mbps downloadlink and a 20 Mbps uplink between the spacecraft and the ground link. The approximate distance for these links is 400 thousands kilometers.

(b) Optically Preamplified Direct Detection Receivers

Optically preamplified direct detection receivers operate through detecting the instantaneous power of the received optical signal and thus have a simpler structure than photon-counting or coherent receivers. These receivers are capable of detecting OOK, differential phase shift keying, and M-ary PPM modulated signals where the data is encoded into the instantaneous optical power [16].

Figure 2.11 shows a general block diagram of optically preamplified direct detection receivers. They consist mainly of an optical preamplifier, optional polarization filter, bandpass optical filter, single photodetector, electrical amplifier, electrical filter, and detection or demodulation circuitry. The optical preamplifier is used especially with a PIN photodetector to improve the sensitivity of the receiver [4]. This amplification process is usually incorporated with the addition of ASE noise components in two polarization modes. The first one is parallel to the incoming optical field and the second one is perpendicular to the incoming optical field. The polarization filter eliminates the perpendicular ASE mode and hence improves the sensitivity of direct detection receivers. The bandpass optical filter suppresses the out-of-band ASE noise and any other background optical noise [4].

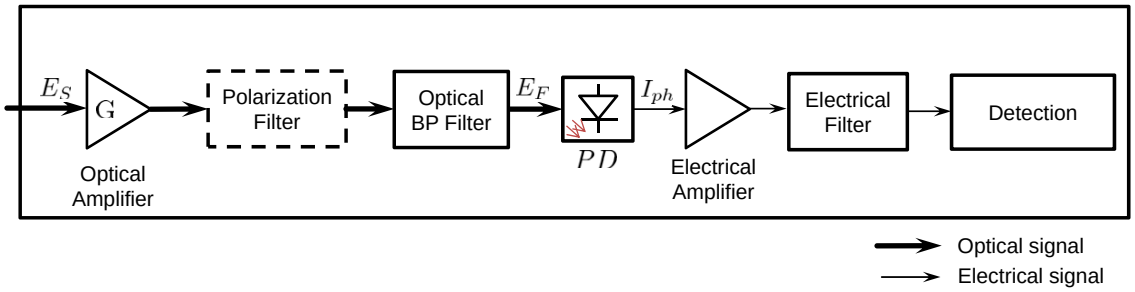

Figure 2.11: A General Block Diagram of Optically Preamplified Direct Detection Receivers.

Noise Statistics in Optically Preamplified Direct Detection Receivers

The electrical field of the received optical signal can be expressed as:

$$E_s = A\cos(2\pi f_{\text{oc}} t), \tag{2.3}$$

where f_{oc} is the optical carrier frequency and A is the amplitude of the incoming optical signal. The optical preamplifier amplifies the signal by a factor of $\sqrt{G}$, where G is the power gain of the amplifier, and adds ASE noise components. The parallel ASE noise ($n_{\|}$) can be considered as a bandpass Gaussian noise with double-sided power spectral density (PSD) given as [66]:

$$N_{ASE} = \frac{1}{2}(G-1)hf_{\text{oc}}n_{sp}, \tag{2.4}$$

where h is the Planck's constant, and n_{sp} is the amplifier noise figure. For ideal amplifiers, the value of n_{sp} is 1 and for typical amplifiers the value of n_{sp} is between 1.4 and 4 [66]. The electrical field of the optical signal after the polarization filter and the bandpass optical filter can be expressed as:

$$\begin{aligned} E_F &= \sqrt{G}A\cos(2\pi f_{\text{oc}}t) + n_{\|F}(t) \\ &= \sqrt{G}A\cos(2\pi f_{\text{oc}}t) + n_{xI}(t)\cos(2\pi f_{\text{oc}}t) - n_{xQ}(t)\sin(2\pi f_{\text{oc}}t), \end{aligned} \tag{2.5}$$

where $n_{\|F}(t)$ is the output noise of the bandpass filter which is modeled as bandpass Gaussian noise. n_{xI} and n_{xQ} are the in-phase and the quadrature-phase components of $n_{\|F}(t)$. The photodetector output which is proportional to the incident optical power is:

$$I_{ph} = \frac{\Re}{2}\left[\left[\sqrt{G}A(t) + n_{xI}(t)\right]^2 + [n_{xQ}(t)]^2\right], \tag{2.6}$$

where $\Re = \eta e/hf_{\text{oc}}$ is the responsivity of the photodetector, e is the electron charge, and η is the quantum efficiency of the photodiode [62]. Due to the square-law nature of the photodetector, the resulting ASE noise will contain two terms which are known as the signal-spontaneous (signal-ASE) and the spontaneous-spontaneous (ASE-ASE) noise terms. The photodetector current of the signal-ASE noise equals:

$$I_{\text{signal-ASE}}(t) = \Re\sqrt{G}An_{xI}(t). \tag{2.7}$$

The double-sided spectral density for the signal-ASE noise term, $S_{\text{signal-ASE}}(f)$, is flat and extends between $-B_0/2$ and $B_0/2$, where B_0 is the bandwidth of the optical bandpass filter, with a constant value of [66]:

$$\begin{aligned} S_{\text{signal-ASE}}(f) &= G(G-1)hf_{\text{oc}}n_{sp}\Re^2A^2 \\ &= 2G(G-1)hf_{\text{oc}}n_{sp}(\frac{e\eta}{hf_{\text{oc}}})^2P_{in} \\ &= 2G(G-1)n_{sp}\frac{e^2}{hf_{\text{oc}}}P_{in}, \end{aligned} \tag{2.8}$$

where $P_{in} = A^2/2$ is the power of the optical signal and η is assumed to be 1. The photodetector current of the ASE-ASE noise term equals:

$$I_{\text{ASE-ASE}}(t) = \frac{\Re}{2}\left(n_{xI}^2(t) + n_{xQ}^2(t)\right). \tag{2.9}$$

The autocorrelation for the random process $n_{xI}^2(t)$ is given by [67, 29]:

$$E\left[n_{xI}^2(t)n_{xI}^2(t+\tau)\right] = R_{n_I}^2(0) + 2R_{n_I}^2(\tau), \tag{2.10}$$

where $R_{n_{xI}}(\tau)$ is the autocorrelation of $n_{xI}(t)$. Since $n_{xI}(t)$ and $n_{xQ}(t)$ are independent random processes, the power spectral density of $I_{\text{ASE-ASE}}(t)$ is twice the power spectral density of the first term in Equation 2.9. Using Equations 2.9 and 2.10, the power spectral density of $I_{\text{ASE-ASE}}(t)$ will include two terms. The first term is an impulse at $f = 0$ with a value of $\frac{1}{2}\left[(G-1)n_{sp}eB_0\right]^2$. The second term has a triangular shape with a maximum power density at $f = 0$ that is equal to $\left[(G-1)n_{sp}e\right]^2 B_0$ and extends from $-B_0$ to B_0. The power spectral densities of $S_{\text{signal-ASE}}$ and $S_{\text{ASE-ASE}}$ are shown in Figure 2.12.

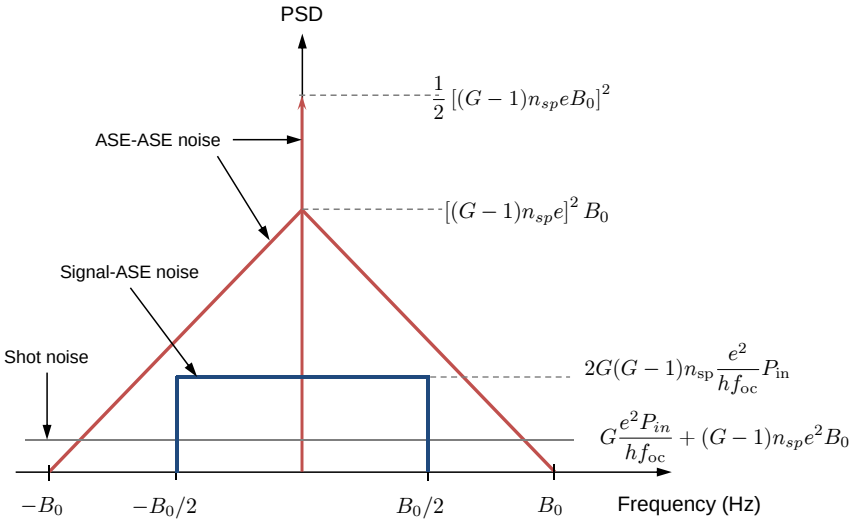

Figure 2.12: Photocurrent Power Spectral Densities.

In addition to ASE optical noise components, electrical noise components such as shot noise and thermal noise exist in optically preamplified direct detection receivers. The

shot noise is generated by the photodetector as a result of the randomness of the electrons flow inside the photodetector [68]. The power spectral density of the shot noise current is given by [29]:

$$\begin{aligned} S_{\text{shot}}(f) &= eR\left[GP_{in} + (G-1)n_{sp}hf_{\text{oc}}\right] \\ &= G\frac{e^2 P_{in}}{hf_{\text{oc}}} + (G-1)n_{sp}e^2 B_0. \end{aligned} \tag{2.11}$$

The power spectral density of the shot noise is also shown in Figure 2.12. The thermal noise results from the Brownian movements of the electrons inside the electrical components. The power spectral density of the thermal noise is assumed to be flat with a typical value of 1 $pA/\sqrt{Hz}$ [29].

In optically preamplified receivers, thermal and shot noise terms are much smaller than the signal-ASE and ASE-ASE noise terms and thus can be neglected. Also, the ASE-ASE noise terms are not Gaussian; thus analytical solutions to their effects on optical systems performance are difficult.

(c) Optical Coherent Receivers

Optical coherent receivers mix a locally generated optical signal with the incoming optical signal before the photo-detection process. The mixing process in optical coherent receivers is equivalent to amplifying the optical signal without noise addition. Detection in optical coherent receivers can be categorized into homodyne detection and hetrodyne detection. In homodyne detection, the frequency of the local oscillator (f_{lo}) should match the frequency of the optical carrier (f_{oc}). The detection in this case is performed at the baseband which reduces the receiver bandwidth and simplifies the detection electronic circuitry [3]. In hetrodyne detection, the mixed signal is down converted into an intermediate frequency $f_{\text{IF}} = f_{\text{oc}} - f_{\text{lo}}$ [69]. Homodyne receivers are more sensitive than optically preamplified direct detection receivers while hetrodyne receivers are equivalent in their performance to optically preamplified direct detection receivers [70].

An advantage of coherent receivers is their capability of detecting the variations in the amplitude, frequency, phase, and polarization of the incoming optical signal. However, the local oscillator optical field should be locked in phase and in polarization to the incoming optical field. This requirement increases the complexity of the receiver design and makes the receiver harder to tolerate [3, 8].

Figure 2.13, shows a simple implementation of coherent receivers known as single branch homodyne receivers. To achieve the optimum mixing, the phase, frequency, and polarization of the local oscillator should be locked to those of the received optical field (E_S). In this configuration, an optical coupler is used to add E_S to the local oscillator field (E_{LO}).

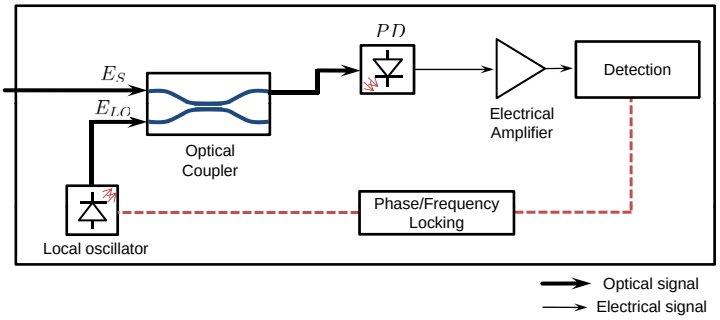

Figure 2.13: Single Branch Homodye Receiver.

The equivalent electrical field of E_S and E_{LO} can be represented as:

$$E_S(t) = A_s(t)\cos\left(2\pi f_{oc}t + \phi_s(t)\right), \tag{2.12}$$

$$E_{LO} = A_l\cos\left(2\pi f_{\text{lo}}t + \phi_{\text{lo}}(t)\right), \tag{2.13}$$

where $A_s(t)$ is the modulated amplitude, $\phi_s(t)$ is the modulated phase, A_l is the amplitude of the local oscillator wave, and $\phi_{\text{lo}}(t)$ is the local oscillator phase shift. At the input of the photodiode, the mixed optical field equals $[E_S(t) + E_{LO}(t)]/\sqrt{2}$. The current of the photodetector is then given by:

$$I(t) = \frac{\Re}{2}\langle[E_S(t) + E_{LO}(t)]^2\rangle, \tag{2.14}$$

where $\Re$ is the photodiode responsivity and the operation $\langle\cdot\rangle$ represents the time average. The beating term of the detection current in Equation (2.14) is the dominant term and can be expressed as:

$$I(t) = \frac{\Re}{2} A_{LO} A_S \cos\left[2\pi f_{IF} t + \phi_S(t)\right]. \tag{2.15}$$

An alternative simple implementation of homodyne coherent receivers, known as the balanced receiver, is shown in Figure 2.14. This configuration increases the received signal power and reduces the local oscillator noise. In balanced receivers, two photodiodes are used where the difference of their currents is used for the detection [30]. The field into the first photodiode is $[E_S(t) + E_{LO}(t)]/\sqrt{2}$, while the field into the second photodiode is $[E_S(t) - E_{LO}(t)]/\sqrt{2}$. The currents of the two photodiodes are:

$$\begin{aligned} I_1(t) &= \frac{\Re_1}{2}\langle[E_S(t) + E_{LO}(t)]^2\rangle, \\ I_2(t) &= \frac{\Re_2}{2}\langle[E_S(t) - E_{LO}(t)]^2\rangle. \end{aligned} \tag{2.16}$$

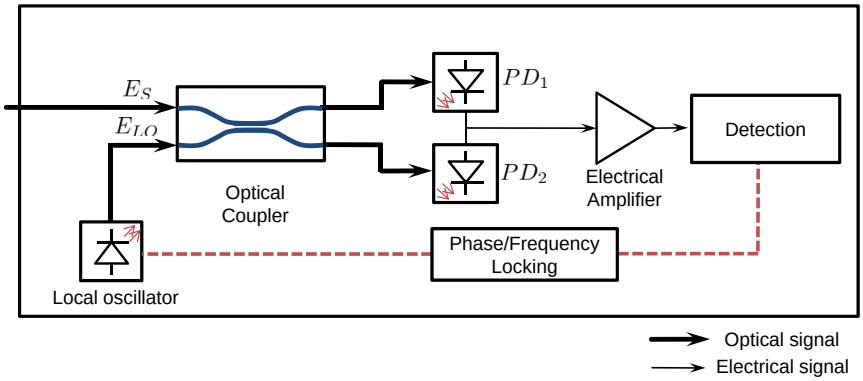

Figure 2.14: Balanced Homodyne Receiver.

Assuming equal responsivities (i.e., $\Re_1 = \Re_2$), the detection current is then:

$$I(t) = \frac{\Re}{2}\left[\langle[E_S(t) + E_{LO}(t)]^2\rangle - \langle[E_S(t) - E_{LO}(t)]^2\rangle\right] \tag{2.17}$$

The beating term of the detection current is the dominant term and can be expressed as:

$$I(t) = \Re A_{lo} A_s(t) \cos\left[2\pi f_{IF} t + \phi_s(t)\right]. \tag{2.18}$$

The block diagram of an optically preamplified homodyne phase/polarization diversity receiver is shown in Figure 2.15. This configuration is capable of separating the in-phase (I) and quadrature-phase (Q) components of two different orthogonal polarizations (e.g., x and y polarizations) of the incoming optical signal.

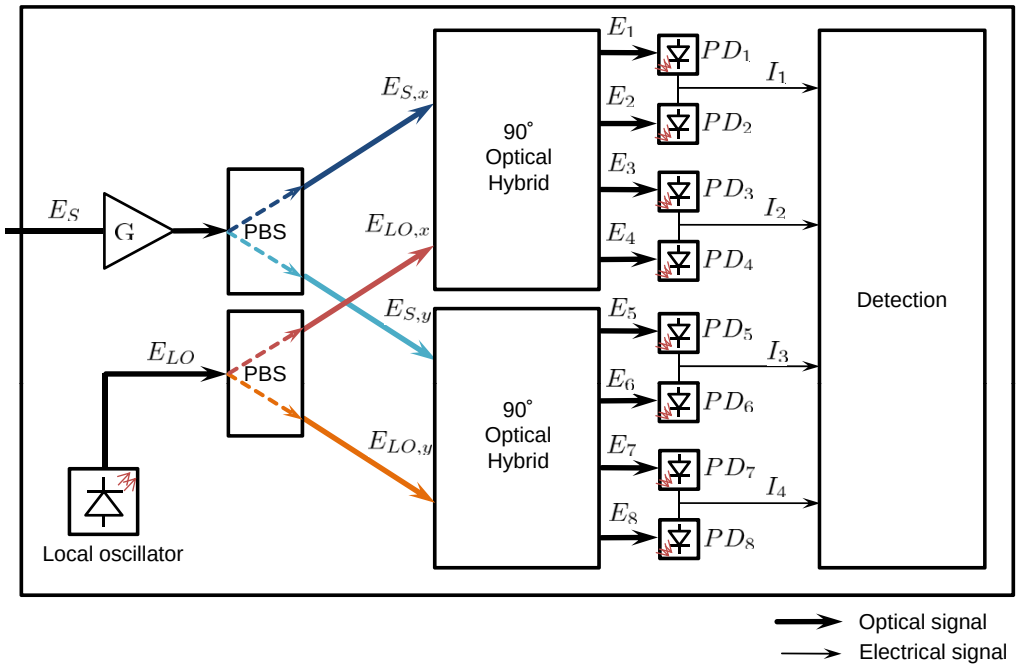

Figure 2.15: Phase/Polarization Diversity Coherent Receiver.

In phase/polarization diversity coherent receivers, two polarization beam splitters (PBS), two 90° optical hybrid devices, and four balanced receivers (i.e., eight photodetectors) are used [69]. The 90° optical hybrid device uses the local oscillator optical signal to internally generate an optical signal with a 90° phase shift. Optical preamplification can be used in coherent detection to increase sensitivity. The phase/polarization coherent receiver in Figure 2.15 utilizes an optical preamplifier to increase sensitivity. The equivalent electrical field of the two ASE noise components can expressed as:

$$\begin{aligned} n(t) &= (n_{xI}(t)\cos(2\pi f_{oc}t) - n_{xQ}(t)\sin(2\pi f_{oc}t)) \\ &+ (n_{yI}(t)\cos(2\pi f_{oc}t) - n_{yQ}(t)\sin(2\pi f_{oc}t))\,, \end{aligned} \tag{2.19}$$

where $n_{xI}(t)$ and $n_{xQ}(t)$ are the in-phase and quadrature-phase components of the ASE noise in the x polarization while $n_{yI}(t)$ and $n_{yQ}(t)$ are the in-phase and quadrature-phase components of the ASE noise in the y polarization. The outputs of the PBSs are:

$$\begin{aligned} E_{S,x}(t) &= (I_x(t) + n_{xI}(t))\cos(2\pi f_{oc}t) - (Q_x(t) + n_{xQ}(t))\sin(2\pi f_{oc}t) \\ E_{S,y}(t) &= (I_y(t) + n_{yI}(t))\cos(2\pi f_{oc}t) - (Q_y(t) + n_{yQ}(t))\sin(2\pi f_{oc}t), \end{aligned} \quad (2.20)$$

where $I_x(t)$ is the incoming signal in-phase component in the x polarization, $Q_x(t)$ is the quadrature-phase component in the x polarization, $I_y(t)$ is the in-phase component in the y polarization, and $Q_y(t)$ is the quadrature-phase component in the y polarization. The outputs of the 90° optical hybrid devices are:

$$\begin{aligned} E_{1,2} &= \frac{1}{2}\left[E_{S,x}(t) \pm A_{lo,x}\cos\left(2\pi f_{lo}t - \phi_{lo}(t)\right)\right], \\ E_{3,4} &= \frac{1}{2}\left[E_{S,x}(t) \pm A_{lo,x}\sin\left(2\pi f_{lo}t - \phi_{lo}(t)\right)\right], \\ E_{5,6} &= \frac{1}{2}\left[E_{S,y}(t) \pm A_{lo,y}\cos\left(2\pi f_{lo}t - \phi_{lo}(t)\right)\right], \\ E_{7,8} &= \frac{1}{2}\left[E_{S,y}(t) \pm A_{lo,y}\sin\left(2\pi f_{lo}t - \phi_{lo}(t)\right)\right], \end{aligned} \quad (2.21)$$

where $A_{lo,x}$ is the local oscillator amplitude in the x polarization, $A_{lo,y}$ is the local oscillator amplitude in the y polarization, $\phi_{lo}(t) = 2\pi\Delta f t + \theta$, $\Delta f = f_{oc} - f_{lo}$, and θ is a random phase shift. The output current of the balanced receives can be given as:

$$\begin{aligned} I_1 &= \Re[\langle E_1^2\rangle - \langle E_2^2\rangle], \\ I_2 &= \Re[\langle E_3^2\rangle - \langle E_4^2\rangle], \\ I_3 &= \Re[\langle E_5^2\rangle - \langle E_6^2\rangle], \\ I_4 &= \Re[\langle E_7^2\rangle - \langle E_8^2\rangle]. \end{aligned} \quad (2.22)$$

I_1 can be expanded as follows:

$$
\begin{aligned}
I_1 &= \Re[\langle E_1^2\rangle - \langle E_2^2\rangle] \\
&= \frac{\Re}{4}\,[\,\langle[E_{S,x}(t) + A_{lo,x}\cos(2\pi f_{lo}t - \phi_{lo}(t))]^2\rangle \\
&\quad -\langle[E_{S,x}(t) - A_{lo,x}\cos(2\pi f_{lo}t - \phi_{lo}(t))]^2\rangle\,] \\
&= \frac{\Re}{4}\,[\,\langle[(I_x(t) + n_{xI} + A_{lo,x}\cos(\phi_{lo}(t)))\cos(2\pi f_{oc}t) - (Q_x(t) + n_{xQ})\sin(2\pi f_{oc}t)]^2\rangle \\
&\quad -\langle[(I_x(t) + n_{xI} - A_{lo,x}\cos(\phi_{lo}(t)))\cos(2\pi f_{oc}t) - (Q_x(t) + n_{xQ})\sin(2\pi f_{oc}t)]^2\rangle.
\end{aligned}
\tag{2.23}
$$

Using the trigonometric equation, $\left[A\cos(x) \pm B\sin(x) = \sqrt{A^2+B^2}\cos(x \mp \tan^{-1}\frac{B}{A})\right]$, I_1 can be expressed as:

$$
I_1 = \Re A_{lo,x}\,[I_x(t) + n_{xI}(t)]\cos(\phi_{lo}(t)) - \Re A_{lo,x}\,[Q_x(t) + n_{xQ}(t)]\sin(\phi_{lo}(t)) \tag{2.24}
$$

Similarly, I_2, I_3, and I_4 can be expressed as:

$$
\begin{aligned}
I_2 &= \Re A_{lo,x}\,[I_x(t) + n_{xI}(t)]\sin(\phi_{lo}(t)) + \Re A_{lo,x}\,[Q_x(t) + n_{xQ}(t)]\cos(\phi_{lo}(t)) \\
I_3 &= \Re A_{lo,y}\,[I_y(t) + n_{yI}(t)]\cos(\phi_{lo}(t)) - \Re A_{lo,y}\,[Q_y(t) + n_{yQ}(t)]\sin(\phi_{lo}(t)) \\
I_4 &= \Re A_{lo,y}\,[I_y(t) + n_{yI}(t)]\sin(\phi_{lo}(t)) + \Re A_{lo,y}\,[Q_y(t) + n_{yQ}(t)]\cos(\phi_{lo}(t))
\end{aligned}
\tag{2.25}
$$

For ideal homodyne phase/diversity receivers, $\phi_{lo}(t) = 0$. The balanced receivers currents are then:

$$
\begin{aligned}
I_1 &= \Re A_{lo,x}\,[I_x(t) + n_{xI}(t)] \\
I_2 &= \Re A_{lo,x}\,[Q_x(t) + n_{xQ}(t)] \\
I_3 &= \Re A_{lo,y}\,[I_y(t) + n_{yI}(t)] \\
I_4 &= \Re A_{lo,y}\,[Q_y(t) + n_{yQ}(t)]
\end{aligned}
\tag{2.26}
$$

which represents the separated I and Q components of the optically preamplified signal in the x polarization and y polarization.

2.3 Link Budget for FSO Systems

Assuming a free-space optical communication system composed of a transmitter and a receiver with a line-of-sight (LOS) and separated with a distance d, Friis free-space transmission equation is typically used to compute the receiver power as follows:

$$P_r = P_t G_t G_r \frac{\lambda^2}{(4\pi)^2 d^2}. \tag{2.27}$$

where, λ is the signal wavelength, P_t is the transmitter power, and G_t, G_r are the transmitter and receiver antenna gains, respectively. Equation 2.27 can also be expressed in terms of the antenna's effective areas defined as:

$$A^{\text{eff}} = \frac{\lambda^2}{4\pi} G, \tag{2.28}$$

in which case, the link budget equation shown in Equation 2.27 becomes:

$$P_r = P_t \frac{\left(4\pi A_t^{\text{eff}}/\lambda^2\right)\left(4\pi A_r^{\text{eff}}/\lambda^2\right)}{(4\pi)^2 d^2/\lambda^2}, \tag{2.29}$$

which yields:

$$P_r = P_t \frac{A_t^{\text{eff}} A_r^{\text{eff}}}{\lambda^2 d^2}. \tag{2.30}$$

The effective area in the above equation is the optical telescope cross-section areas [8, 16, 28, 71]. A^{eff} of the transmitter and the receiver can be expressed in terms of the diameter (D) and the efficiency (η) as follows:

$$A^{\text{eff}} = \frac{\pi D^2}{4} \eta. \tag{2.31}$$

Assuming a free-space optical communication system operating at 1.55μm wavelength with optical telescope diameters (D) of 0.16 m [21] or 0.2, transmitter and receiver telescope efficiency η of 0.5, average optical power of 1 W, and at a distance of 40,000 km, the minimum required E_b/N_0 to achieve the link is:

$$E_b/N_0 = \frac{P_r \times T_b}{h f_{oc} n_{sp}}. \tag{2.32}$$

Table 2.1 summarizes the minimum required E_b/N_0 for different bit rates, telescope diameters, and values of n_{sp}.

Table 2.1: Link Budget Estimation.

	D=0.16 m		**D=0.2 m**	
	10 Gbps	40 Gbps	10 Gbps	40 Gbps
$n_{sp} = 1$	13.12 dB	7.1 dB	17 dB	10.98 dB
$n_{sp} = 3$	8.35 dB	2.33 dB	12.23 dB	6.21 dB

From Table 2.1, if an FSO system provides a BER of 10^{-3} at an E_b/N_0 value of 12 dB, it can be concluded that the only achievable link is the 10 Gbps link with $D = 0.16$ and $n_{sp} = 1$. This link has a margin of 1.12 dB. For another FSO system that provides a BER of 10^{-3} at an E_b/N_0 value of 7 dB, the same link is achievable with a margin of 6.12 dB. Also a 10 Gbps link with $D = 0.16$ and $n_{sp} = 3$ is possible with a margin of 1.35 dB.

Chapter 3

Performance Evaluation of Optically Preamplified NRZ-OOK Systems

In this chapter, the theoretical performance of optically preamplified NRZ-OOK systems that employ optical matched-filters and are affected by one or two ASE noise sources is discussed. Monte-Carlo simulations using MATLAB were used to evaluate the BER performance of these systems in addition to systems using non-matched filters such as Fabry-Pérot filters. In the rest of this chapter, the simulation model is discussed as well as the BER results.

3.1 Theoretical Performance of Optically Preamplified NRZ-OOK Systems

In non-coherent detectors with optical matched-filters, the received NRZ-OOK signal amplitude (r) at the decision sample has a probability density function (PDF) given by [72]:

$$f_1(r) = \frac{r}{\sigma_n^2} I_0\left(\frac{rA}{\sigma_n^2}\right) \exp\left(-\frac{r^2+A^2}{2\sigma_n^2}\right) \qquad \text{for } s_1, \tag{3.1}$$

and

$$f_0(r) = \frac{r}{\sigma_n^2} \exp\left(-\frac{r^2}{2\sigma_n^2}\right) \qquad \text{for } s_0, \tag{3.2}$$

where A is the maximum output of the matched filter, σ_n^2 is the variance of the noise, $f_1(r)$ and $f_0(r)$ are the PDFs when the transmitted bits are "1" and "0", respectively, and I_0 is

the 0^{th} order modified Bessel function of the first kind. $f_1(r)$ and $f_0(r)$ are the Rice and Rayleigh distributions, respectively [72].

In NRZ-OOK, a threshold (r_{thr}) is required to decide on the received bit. If the value of the decision sample r is larger than r_{thr}, the detector decides that "1" was transmitted and if r is less than r_{thr}, the detector decides that "0" was transmitted. For equally likely binary outputs, the BER is:

$$\text{BER}_{\text{OOK}} = \frac{1}{2}\int_{r_{\text{thr}}}^{\infty} f_0(r)dr + \frac{1}{2}\left[1 - \int_{r_{\text{thr}}}^{\infty} f_1(r)dr\right]. \tag{3.3}$$

The BER expression can be written in terms of A, r_{thr} and σ_n by substituting Equations 3.1 and 3.2 into 3.3 and by using the Marcum's Q-function defined as:

$$\text{Q}\left(a,b\right) = \begin{cases} \exp(-\frac{a^2+b^2}{2}) \sum\limits_{k=0}^{\infty} \left(\frac{a}{b}\right)^k I_k\left(ab\right), & a \leq b \\ 1 + \exp(-\frac{a^2+b^2}{2}) I_0(ab) - \exp(-\frac{a^2+b^2}{2}) \sum\limits_{k=0}^{\infty} \left(\frac{a}{b}\right)^k I_k\left(ab\right) & a > b \end{cases} \tag{3.4}$$

The BER_{OOK} is then given by [30]:

$$\text{BER}_{\text{OOK}} = \frac{1}{2}\left[1 - Q\left(\frac{A}{\sigma_n}, \frac{r_{\text{thr}}}{\sigma_n}\right)\right] + \frac{1}{2}\exp\left(-\frac{r_{\text{thr}}^2}{2\sigma_n^2}\right). \tag{3.5}$$

The optimum threshold r_{thr} can be obtained by solving [$d/d_{r_{\text{thr}}}\left(\text{BER}_{\text{OOK}}\right)$=0] to get [30]:

$$I_0\left(\frac{Ar_{thr}}{\sigma_n^2}\right)\exp\left(-\frac{A^2}{2\sigma_n^2}\right) = 1 \tag{3.6}$$

Note that for optical matched-filters [72]:

$$\left(\frac{A}{\sigma_n}\right)^2 = 4E_b/N_0, \tag{3.7}$$

where E_b is the average energy per bit and N_0 is the effective single-sided power spectral density of the noise [72]. In this case, the BER and the optimum threshold expression in

terms of E_b/N_0 is given by:

$$\text{BER}_{\text{OOK}} = \frac{1}{2}\left[1 - Q\left(2\sqrt{E_b/N_0}, 2\alpha_{\text{thr}}\sqrt{E_b/N_0}\right)\right] + \frac{1}{2}\exp\left(-2\alpha_{\text{thr}}^2 E_b/N_0\right), \quad (3.8)$$

and

$$I_0\left(4\alpha_{\text{thr}}E_b/N_0\right)\exp\left(-2E_b/N_0\right) = 1, \quad (3.9)$$

where $\alpha_{\text{thr}} = r_{\text{thr}}/A$. Equations 3.8 and 3.9 can be used for optically preamplified NRZ-OOK direct detection systems with matched filters and affected by 1 ASE noise component [30, 69]. In [72], an approximate BER expression for non-coherent OOK systems is provided through Gaussian approximation for $f_1(r)$ and by assuming a fixed threshold r_{thr} at E_b. For $E_b/N_0 \gg 1$, the BER_{OOK} is approximated by:

$$\text{BER}_{\text{OOK}} \approx \frac{1}{2}e^{-\frac{1}{2}E_b/N_0}. \quad (3.10)$$

Optically preamplified NRZ-OOK direct detection systems with matched-filters and affected by 2 ASE noise components have the following PDF for the received NRZ-OOK signal power (r):

$$f_1(r) = \frac{1}{2\sigma_n^2}\sqrt{\frac{r}{A^2}}\exp\left(-(A^2+r)/2\sigma_n^2\right) I_1\left(\sqrt{r}\frac{A}{\sigma_n^2}\right), r \geq 0 \quad \text{for } s_1, \quad (3.11)$$

$$f_0(r) = \frac{r}{4\sigma_n^4}\exp\left(-r/2\sigma_n^2\right), r \geq 0 \quad \text{for } s_0, \quad (3.12)$$

where I_1 is the 1^{st} order modified Bessel function of the first kind. f_1 follows the non-central chi-square (χ^2) distribution with four degrees of freedom while f_0 is Gamma distributed [30].

The BER expression can be written in terms of A, r_{thr}, and σ_n using Equations 3.11 and 3.12 and by using the second-order generalized Marcum's Q-function defined as:

$$Q_2\left(a, b\right) = Q\left(a, b\right) + \frac{b}{a}e^{-(a^2+b^2)/2}I_1(ab). \quad (3.13)$$

Then, $\mathrm{BER}_{\mathrm{OOK-2ASE}}$ can be expressed as:

$$\mathrm{BER}_{\mathrm{OOK-2ASE}} = \frac{1}{2}\left[1 - Q_2\left(\frac{A}{\sigma_n}, \frac{\sqrt{y_{\mathrm{thr}}}}{\sigma_n}\right)\right] + \frac{1}{2}\exp\left(-\frac{y_{\mathrm{thr}}}{2\sigma_n^2}\right)\left(1 + \frac{y_{\mathrm{thr}}}{2\sigma_n^2}\right). \quad (3.14)$$

The optimum threshold r_{thr} can be obtained by solving $[d/d_{r_{\mathrm{thr}}}\left(\mathrm{BER}_{\mathrm{OOK-2ASE}}\right)$=0] to get:

$$\sqrt{r_{\mathrm{thr}}}\frac{A}{2\sigma_n^2} = e^{-A^2/2\sigma_n^2} I_1\left(\sqrt{r_{\mathrm{thr}}}\frac{A}{\sigma_n^2}\right), r \geq 0. \quad (3.15)$$

The BER and the optimum threshold expression in terms of E_b/N_0 is given by:

$$\begin{aligned} \mathrm{BER}_{\mathrm{OOK-2ASE}} &= \frac{1}{2}\left[1 - Q_2\left(2\sqrt{E_b/N_0}, 2\sqrt{\gamma_{\mathrm{thr}} \times E_b/N_0}\right)\right] \\ &+ \frac{1}{2}\exp\left(-2\gamma_{\mathrm{thr}}E_b/N_0\right)\left(1 + 2\gamma_{\mathrm{thr}}E_b/N_0\right), \end{aligned} \quad (3.16)$$

and

$$I_1\left(4\gamma_{\mathrm{thr}}E_b/N_0\right)\exp\left(-2E_b/N_0\right) = 2\sqrt{\gamma_{\mathrm{thr}}}E_b/N_0, \quad (3.17)$$

where $\gamma_{\mathrm{thr}} = r_{\mathrm{thr}}/A^2$.

Note that the BER expressions and optimum threshold equations provided above are limited only to NRZ-OOK systems with optical matched-filters. Several studies for optically preamplified OOK systems have used the Gaussian approximation to evaluate the BER performance. In [73], the Gaussian approximation results were compared to the exact results obtained through the Marcum Q function for OOK, DPSK, and FSK systems using matched-filters. The study in [74] also used the Gaussian approximation to analyze the effects of the amplifier noise and the linewidth of the laser in addition to the bandwidth of the bandpass optical filter and the bit rate on optically preamplified systems.

The performance of practical OOK systems employing non-matched realistic optical filters such as the Fabry Pérot filter have been addressed in many studies. In [17], the performance of optically preamplified NRZ and RZ OOK systems was evaluated at a BER of 10^{-9} using the Gaussian approximation and quasi analytical methods. This study considered and optimized two types of optical filters, namely the Fabry Pérot and Bragg Grating

with 5^{th} order Butterworth electrical filters. The effects of pulse shaping and system imperfections such as ISI, extinction ratio, frequency chirp, and frequency drift were also addressed. In [75], a closed form expression for the moment generating function (MGF) for the decision samples was derived and used to evaluate the performance of optically preamplified OOK systems with Fabry Pérot filters. The study in [76] presented experimental and numerical investigations for the effects of varying the bandwidths of the optical and electrical filters on the performance of 10 Gbps optically preamplified NRZ and RZ OOK systems. Optical and electrical filter optimization was also addressed in [77] and recently in [78]. In [77], the exact mean and variance of the noised signal were used to obtain another Gaussian approximation. This approximation allowed for the performance evaluation of systems with arbitrary filters. The study in [78] used the Fourier series expansion methods to evaluate the exact BER.

In this chapter, Monte-Carlo simulations were used to evaluate the performance of NRZ-OOK systems including the Fabry Pérot filter, dual polarization noise, and finite extinction. Unlike, previous studies and due to the advances in FEC [79], the system performance is provided in terms of the receiver sensitivity at BER values of 10^{-3} and 10^{-4}. The following sections provide the details of the simulation model and the obtained results.

3.2 Optically Preamplified NRZ-OOK Receiver Simulation Model

Figure 3.1 illustrates the simulation model used for the optically preamplifed NRZ-OOK receiver. In this model, the lowpass equivalent electrical field of the received NRZ-OOK signal is applied to the receiver input where the pulse shape was assumed to be rectangular. The input field $E_{\text{in}}(t)$ is amplified by the optical amplifier and corrupted by the amplifier output noise, $n(t)$, which has two components. The polarization of the first component of the noise, denoted by $n_{\parallel}(t)$, is parallel to the input field polarization, and the polarization of the second component, denoted by $n_{\perp}(t)$, is perpendicular to the input field polarization. Each of the $n_{\parallel}(t)$ and $n_{\perp}(t)$ is modeled as a complex Gaussian noise process. The real and the imaginary parts of this process have a zero mean and power

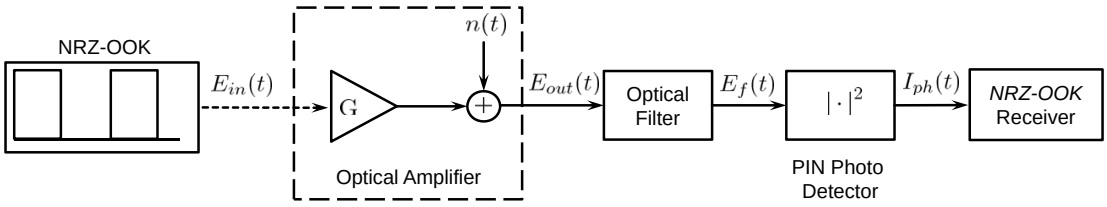

Figure 3.1: Optically Preamplified NRZ-OOK Receiver Model.

spectral density N_{ASE} equal to $n_{sp}hf(G-1)$, which is also equal to $N_0(G-1)$, where N_0 is the single-sided power spectral density of the amplifier equivalent input noise, G is the amplifier power gain, n_{sp} is the amplifier noise figure, h is Plank's constant, and f is the optical frequency. The amplifier output field is given by:

$$E_{\text{out}}(t) = E_{\text{in}}(t)\sqrt{G} + n_{\parallel}(t) + n_{\perp}(t) \tag{3.18}$$

The amplifier output field is then passed through the optical filter, the output of which is given by:

$$E_f(t) = \Big(E_{\text{in}}(t)\sqrt{G} + n_{\parallel}(t)\Big) * h(t) + n_{\perp}(t) * h(t) \tag{3.19}$$

The filter output is then applied to a PIN photodiode to generate an electrical current I_{ph} that is given by:

$$I_{ph}(t) = \Big|\Big(E_{in}(t)\sqrt{G} + n_{\parallel}(t)\Big) * h(t)\Big|^2 + |n_{\perp}(t) * h(t)|^2 \tag{3.20}$$

where $h(t)$ is the impulse response of the optical filter and "$*$" denotes linear convolution. The electrical current $I_{ph}(t)$ is directly connected to an ideal NRZ-OOK receiver where the BER is calculated. The receiver used in this model uses an optimum decision threshold at each value of E_b/N_0.

3.3 Optically Preamplified NRZ-OOK Simulation Results

Our simulations considered different scenarios. First, we simulated a system with an optical matched-filter in the presence of one ASE noise component. Second, the same

system was simulated in the presence of two ASE noise components, namely $n_{\parallel}$ and $n_{\perp}$. To ensure the accuracy of the simulation results, more than 100 errors per each evaluation were generated. For example, for a BER of 10^{-4}, more than 10^6 bits were simulated. The optimum threshold at each E_b/N_0 value was determined through simulations in steps of 5% of the maximum optical power. Figure 3.2 shows the optimum thresholds obtained through simulation and through numerical solutions of the analytical expressions in Equations 3.9 and 3.17. For low E_b/N_0 values (E_b/N_0 less than 3 dB), our simulations showed that the BER performance is not sensitive to the threshold used. On the other hand, for higher E_b/N_0 values, the BER performance is more sensitive to the threshold and matches the analytical results as can be seen in Figure 3.2.

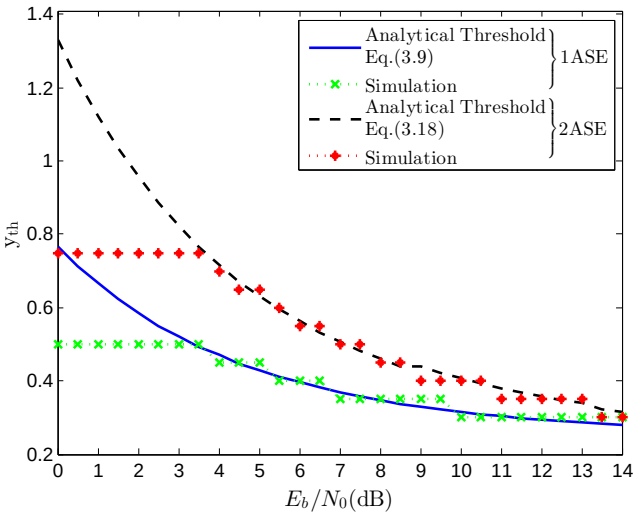

Figure 3.2: Optimum Thresholds for Matched-Filter NRZ-OOK Systems.

3.3.1 Optical Matched-Filter Results

Figure 3.3 shows the BER results for systems employing a matched-filter, affected by one ASE noise component, and using the simulation-based thresholds at each E_b/N_0. The optical matched-filter has a rectangular impulse response with a width equal to the bit time. Theoretical and approximated curves in Figure 3.3 represent Equations 3.8 and 3.10, respectively. Simulation results were found to match the theoretical BER, which validates the model.

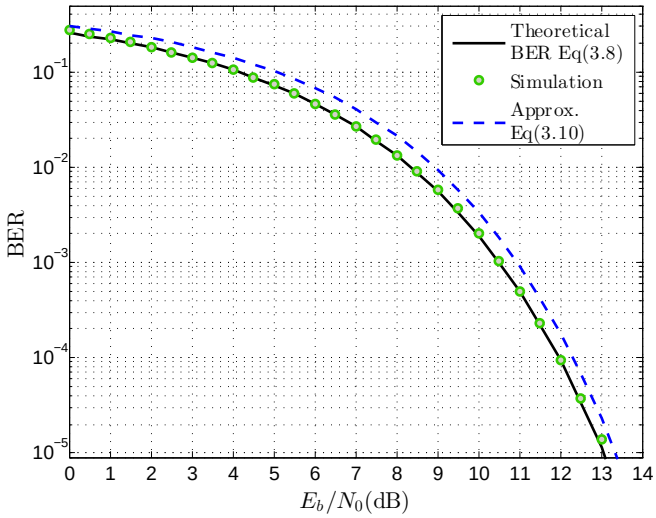

Figure 3.3: Theoretical and Approximated BER for Optical Matched-Filter NRZ-OOK Systems with 1 ASE Noise Source.

Figure 3.4 shows the BER results for systems with an optical matched-filter and affected by two ASE noise sources. The theoretical curve in Figure 3.4 represents Equation 3.16. Simulation results for the systems with a matched-filter, that add two complex noise components ($n_{\|}$, and $n_{\perp}$) and use the simulation-based optimum thresholds determined at each E_b/N_0 are also shown. Simulation results are identical to the theoretical BER expression for two ASE noise sources.

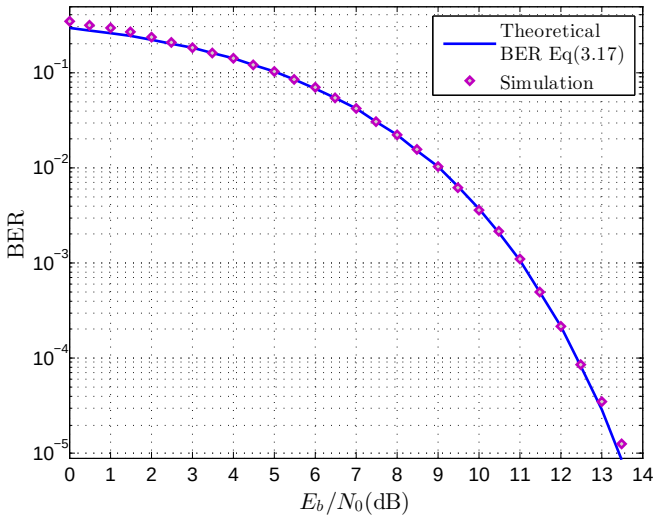

Figure 3.4: Theoretical BER for Matched-Filter NRZ-OOK Systems with 2 ASE Noise Sources.

3.3.2 Fabry Pérot Filters Results

To evaluate the performance of NRZ-OOK systems that use practical optical filters, the matched filter was replaced by a Fabry Pérot filter. Simulation results were obtained assuming no electrical filter at the receiver. To determine the optimum full width half maximum (FWHM) bandwidth of the Fabry-Pérot filter, simulations were carried out for a range of FWHM values starting from $0.2R_b$ to $1R_b$ in steps of $0.1R_b$, where R_b is the bit rate in bits/sec. It was noticed that the optimum thresholds varied by changing the FWHM value of the Fabry Pérot filter. Thus, at each value of the FWHM, the optimum thresholds at each E_b/N_0 value were obtained and used. Figure 3.5 shows the BER results for the matched-filter while considering one ASE and two ASE noise sources and for three values of the FWHM for the Fabry-Pérot filter while considering two ASE noise sources. The

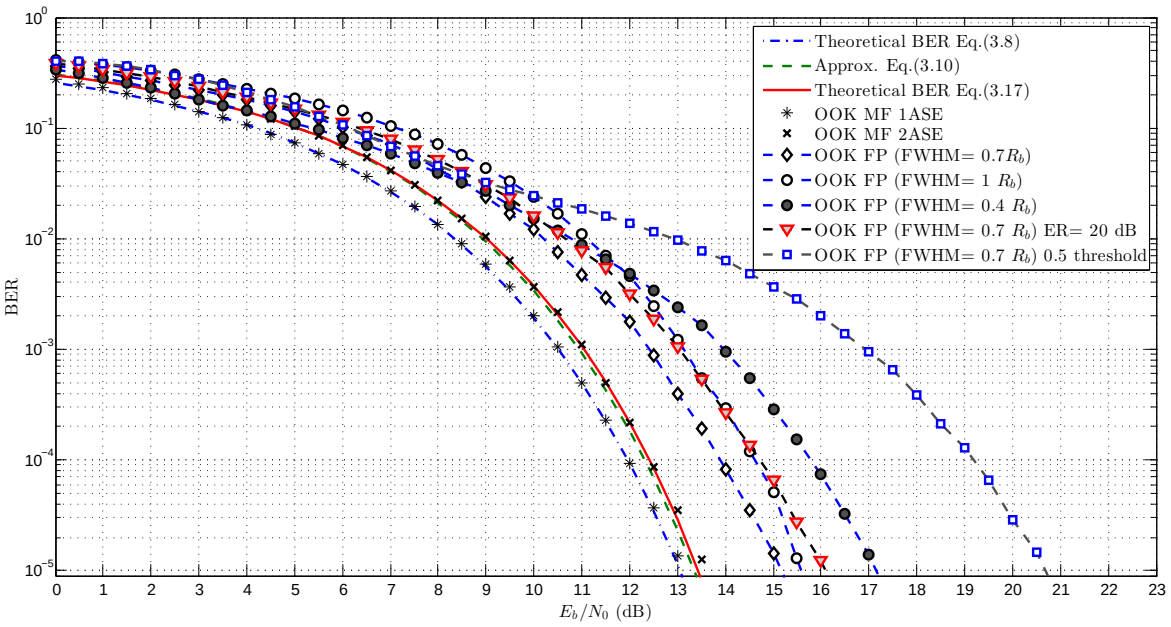

Figure 3.5: BER Results for Optically Preamplified NRZ-OOK Systems.

three values are $0.4R_b$, $0.7R_b$, and $1R_b$, respectively. As shown in Figure 3.5, the optimal FWHM value is $0.7R_b$ which provided an E_b/N_0 value of 12.4 dB at a BER of 10^{-3}. The results presented in Figure 3.5 are summarized in Table 3.1 in terms of E_b/N_0 as well as required photons per bit (PPB) for $n_{sp} = 1$ (ideal case) and $n_{sp} = 3$.

Table 3.1: Performance of Optically Preamplified NRZ-OOK Systems at a BER of 10^{-3} and 10^{-4}.

Performance	BER	MF$*$ 1 ASE ER = ∞	MF 2 ASE ER = ∞	Theoretical Approx. ER = ∞	FP‡ ($0.4R_b$) 2 ASE ER = ∞	FP ($0.7R_b$) 2 ASE ER = ∞	FP ($1R_b$) 2 ASE ER ∞	FP ($0.7R_b$) 2 ASE ER = 20 dB	FP($0.7R_b$) 2 ASE ER = 20 dB§
E_b/N_0 (dB)	10^{-3}	10.53	11.05	10.95	13.95	12.4	13.13	13.05	16.9
PPB ($n_{sp}=1$)		11.3	12.7	12.4	24.8	17.37	20.56	20.18	49
PPB ($n_{sp}=3$)		34	38.2	37.3	74.5	52	61.68	60.55	147
$E_b/N_0(dB)$	10^{-4}	11.96	12.42	12.3	15.8	13.9	14.6	14.7	19.2
PPB ($n_{sp}=1$)		15.7	17.46	17	38	24.55	28.84	29.5	83.18
PPB ($n_{sp}=3$)		47.11	34.92	51	114	73.64	86.5	88.5	250

$*$ Matched Filter

‡ Fabry Pérot

§ For fixed threshold at 50% of the maximum received optical power.

The extinction ratio (ER) in NRZ-OOK systems is the ratio of the optical power when "1" is transmitted to the optical power when "0" is transmitted. The impact of the ER on the performance of systems with Fabry Pérot filters were also considered in our simulations. Under an ER of 20 dB, an E_b/N_0 of approximately 13.05 dB is required for a BER of 10^{-3}. The optimum thresholds when the ER is 20 dB were found to be different than the optimum thresholds in the case of no extinction (ER = ∞) and were obtained at each E_b/N_0 value. Finally, the BER results for systems using an optimum Fabry Pérot filter under 20 dB ER were also generated using a constant threshold at 50% of the maximum received optical power. Systems using a constant threshold are more practical than those using variable thresholds but noticeably, the latter reduce the sensitivity of the receiver. The required E_b/N_0 in this case is 16.9 dB at a BER of 10^{-3} which is worse than the optimum threshold results by 3.85 dB. Table 3.1 summarizes the simulation results for the optically preamplified OOK systems considered in this study. The required PPB values are calculated for the E_b/N_0 (dB) values as follows:

$$\text{PPB} = n_{sp} \times E_b/N_0, \tag{3.21}$$

where E_b/N_0 is in linear units, $N_0 = hf_o n_{sp}$ and hf_o is the energy of a single photon.

As seen in Table 3.1, optically preamplified OOK systems affected by two ASE noise sources and using an optimum FWHM of $0.7R_b$ for the Fabry Pérot filter require a

minimum E_b/N_0 of 13.05 dB and 16.9 dB for the cases of the optimized and the fixed thresholds, respectively. As seen in Table 2.1, the only achievable link for the case of the optimum threshold is the link with a bit rate of 10 Gbps and a value for $n_{sp} = 1$, where the margin is 0.07 dB, and 3.95 dB for the cases of an optical antenna diameter of 0.16 and 2 m, respectively.

Chapter 4

Performance Evaluation of Optically Preamplified Direct Detection 16- and 64-ary PPM Systems

In this chapter, the performance of optically preamplified direct detection 16-ary and 64-ary PPM systems is evaluated. The selection of the modulation level (M) for optically preamplified M-ary PPM systems is based on a trade-off between the desired performance and the available receiver bandwidth. It will be shown that in M-ary PPM orthogonal modulation schemes, increasing M reduces the required E_b/N_0 to achieve a certain BER and hence increases the sensitivity. However, increasing M increases the bandwidths of the optical and electrical filters.

MATLAB-based Monte-Carlo simulations were used to evaluate the BER without assuming that the noise at the decision sample was Gaussian. The combined effects of the dual polarized amplifier noise, the Fabry Pérot optical filter, the extinction ratio of the optical transmitter, and the electric filtering at the receiver are all considered. Extensive simulations were carried out to optimize the bandwidths of the optical and electrical filters at the receiver. Sensitivity degradations due to finite extinction ratios in the 16-ary and the 64-ary PPM systems with two different pulse shapes are studied. Furthermore, the performance penalties due to frequency drift and timing jitter at the receiver are calculated.

4.1 Theoretical Performance of Optically Preamplified M-ary PPM Systems

The BER performance of optically preamplified M-ary PPM systems using optical matched-filters can be obtained by using the PDFs of the received optical power in NRZ-OOK systems provided in Chapter 3 and following the analysis in [71]. The PDF of the output of the matched-filter for bit "1", $f_1(\upsilon)$, in OOK systems can be used to represent the PDF of the output of the matched-filter for the slot that contains the optical pulse in the M-ary PPM systems. The PDF of the output of the matched-filter for bit "0", $f_0(\upsilon)$, can be used to represent the PDF of the output of the matched-filter in the remaining $(M-1)$ empty slots. For systems affected by one ASE noise source, $f_1(\upsilon)$ and $f_0(\upsilon)$ can be expressed as [69]:

$$f_1(\upsilon) = 2\upsilon E_s/N_0 \times I_0(2\upsilon E_s/N_0) \exp\left(-(\upsilon^2+1)E_s/N_0\right). \tag{4.1}$$

$$f_0(\upsilon) = 2\upsilon E_s/N_0 \exp\left(-\upsilon^2 E_s/N_0\right). \tag{4.2}$$

The symbol error probability (SER) can be obtained by calculating the probability that at least one of the empty slots has a noise power (υ_e) higher than υ, given that the received optical power (υ_f) in the filled slot is equal to υ. Assuming that the noise power in the empty slots are independent, we have:

$$P(\upsilon_e > \upsilon | \upsilon_f = \upsilon) = 1 - P(\upsilon_e < \upsilon | \upsilon_f = \upsilon)^{(M-1)}. \tag{4.3}$$

Then, the probability that at least one empty slot has optical power higher than (υ) is:

$$P(\upsilon_e > \upsilon) = \int_{\upsilon=0}^{\infty} P[\upsilon_e > \upsilon | \upsilon_f = \upsilon] \times P[\upsilon_f = \upsilon]\, d\upsilon, \tag{4.4}$$

Using the PDF in Equation 4.2, the term $P(\upsilon_e < \upsilon | \upsilon_f = \upsilon)$ in Equation 4.4 can be expressed as:

$$P(\upsilon_e < \upsilon | \upsilon_f = \upsilon) = 1 - \int_{y=\upsilon}^{\infty} 2yE_s/N_0 \exp\left(-y^2 E_s/N_0\right) dy. \tag{4.5}$$

The right term in the integration in Equation 4.4 equals the PDF in Equation 4.1. and the left term can be expressed in terms of E_s/N_0 as follows:

$$P(\upsilon_e > \upsilon | \upsilon_f = \upsilon) = 1 - \left(1 - \int_{y=\upsilon}^{\infty} 2yE_s/N_0 \exp\left(-y^2 E_s/N_0\right) dy\right)^{(M-1)}.$$

Then, the symbol error ratio (SER) of optically preamplified M-ary PPM systems affected by one ASE noise can be formulated as:

$$\begin{aligned}&\text{SER}_{M-\text{PPM-1ASE}} = \\ &\int_{\upsilon=0}^{\infty} \left[1 - \left(1 - \int_{y=\upsilon}^{\infty} 2yE_s/N_0 \exp\left(-y^2 E_s/N_0\right) dy\right)^{(M-1)}\right] \\ &\times 2\upsilon E_s/N_0 \times I_0\left(2\upsilon E_s/N_0\right) \exp\left(-(\upsilon^2+1)E_s/N_0\right) d\upsilon. \end{aligned} \tag{4.6}$$

The BER of M-ary systems can be related to the SER as follows [16, 71]:

$$\text{BER}_{M-\text{ary}} = \frac{2^{r-1}}{2^r - 1}\text{SER}_{M-\text{ary}} = \frac{M}{2(M-1)}\text{SER}_{M-\text{ary}}, \quad r = \log_2 M. \tag{4.7}$$

Equation 4.6 has a closed form expression provided in [71] as the theoretical BER performance of non-coherent detection of orthogonal modulation schemes. The bit error ratio is given by:

$$\text{BER}_{\text{M-ary}} = \frac{2^{r-1}}{2^r - 1} \sum_{n=1}^{M-1} \frac{(-1)^{n+1}}{n+1} \binom{M-1}{n} \exp\left[-\frac{nr}{n+1} E_b/N_0\right]. \tag{4.8}$$

For systems affected by two ASE noise sources, $f_1(\upsilon)$ and $f_0(\upsilon)$ as a function of E_s/N_0 can be expressed as:

$$f_1(\upsilon) = \sqrt{\upsilon} E_s/N_0 \times I_1\left(2\sqrt{\upsilon} E_s/N_0\right) \exp\left(-(\upsilon+1)E_s/N_0\right). \tag{4.9}$$

$$f_0(\upsilon) = 2\upsilon E_s/N_0 \exp\left(-\upsilon E_s/N_0\right). \tag{4.10}$$

Then, the SER of optically preamplified M-ary PPM systems affected by two ASE noise

sources can be formulated as:

$$\begin{aligned}&\text{SER}_{\text{M-PPM-2ASE}} = \\ &\int_{\upsilon=0}^{\infty}\left[1-\left(1-\int_{y=\upsilon}^{\infty} yE_s/N_0 \times \exp\left(-yE_s/N_0\right)dy\right)^{(M-1)}\right] \\ &\times\sqrt{\upsilon}E_s/N_0 \times I_1\left(2\sqrt{\upsilon}E_s/N_0\right)\exp\left(-(\upsilon+1)E_s/N_0\right)d\upsilon. \end{aligned} \tag{4.11}$$

The SER expressions provided by Equations 4.6 and 4.11 are limited to M-ary PPM systems with matched-filters. Gaussian approximations were used in [38, 42, 43, 44] to evaluate and analyze the BER performance of optically preamplified M-ary PPM systems.

Theoretical BER performance of optically preamplified M-ary PPM systems using matched-filters and affected by one ASE noise source (i.e. $n_{\parallel}$) and two ASE noise sources (i.e. $n_{\parallel}$ and $n_{\perp}$) for $M \in [4, 8, 16, 32, 64]$ are shown in Figures 4.1 and 4.2, respectively. Equation 4.6 and 4.11 were numerically evaluated to obtain the SER results. The BER results are obtained through Equation 4.7 and are provided as a function of E_b/N_0 where for M-ary systems, E_b/N_0 is related to E_s/N_0 as follows:

$$E_s/N_0 = (\log_2(M)) \times E_b/N_0. \tag{4.12}$$

Comparing the results in Figure 4.1 and Figure 4.2, it is noticed that systems affected by two ASE noise sources have a degradation of approximately 0.5 dB relative to systems affected by only one ASE noise source.

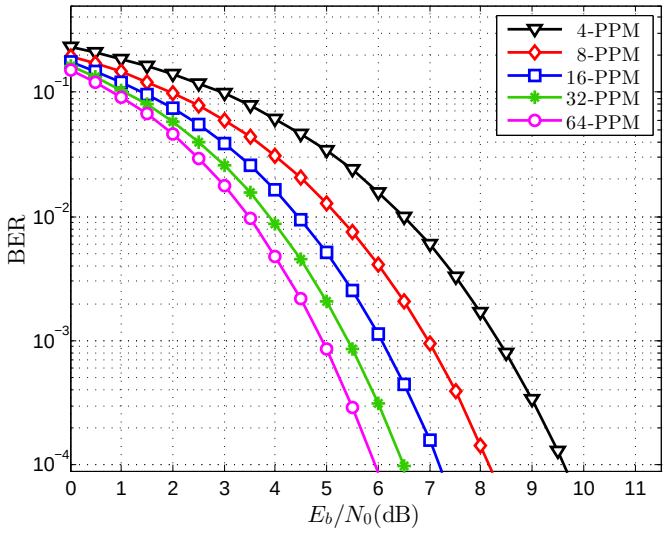

Figure 4.1: Theoretical BER for Optically Preamplified M-ary PPM Systems Affected by 1 ASE Using Only an Optical Matched-Filter.

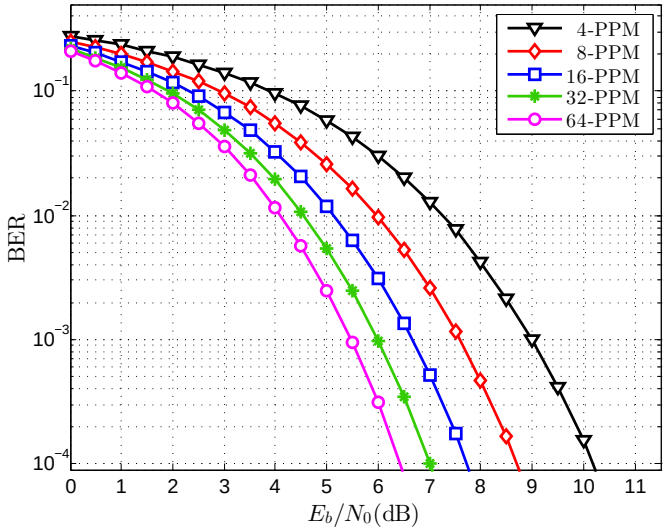

Figure 4.2: Theoretical BER for Optically Preamplified M-ary PPM Systems Affected by 2 ASE Using Only an Optical Matched-Filter.

4.2 Optically Preamplified M-ary PPM Receiver Simulation Model

Figure 4.3 represents the simulation model for an optically preamplified M-ary PPM receiver. In M-ary PPM systems, each symbol is divided into M slots of equal

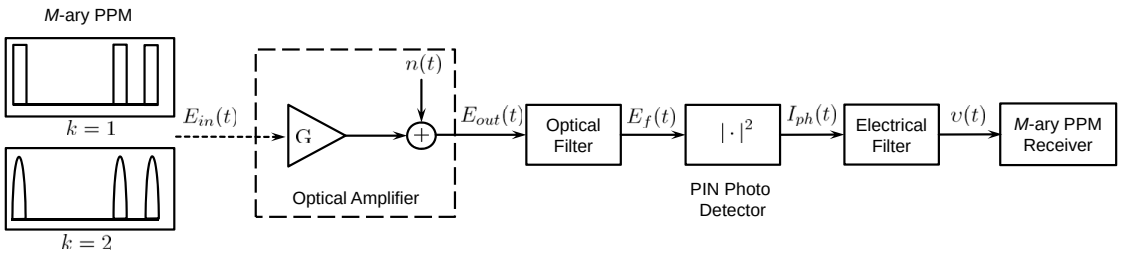

Figure 4.3: Optically Preamplified M-ary PPM Receiver Model.

durations to represent $r = \log_2(M)$ bits. Based on the transmitted r bits, an optical pulse will be located in one of the M slots. The lowpass equivalent electrical field of the M-ary PPM, ($E_{in}(t) = \sqrt{p(t)}$), is applied to the receiver input where the power waveform of the optical pulse $p(t)$ can be expresses as:

$$p(t) = \begin{cases} \frac{1}{2}P_{\max}(1-\delta^2)\left[1-\sin\left(\frac{\pi k}{(k-1)T_s}\left(\left|t-\frac{T_s}{2}\right|-\frac{T_s}{2k}\right)\right)\right]+\delta^2 \\ \qquad\qquad t \in \left[0, \frac{k-1}{k}T_s\right] \text{ and } \left[\frac{1}{k}T_s, T_s\right] \\ P_{\max}, \qquad\qquad t \in \left[\frac{k-1}{k}T_s, \frac{1}{k}T_s\right] \end{cases}, \tag{4.13}$$

where T_s is the slot duration, P_{max} is the maximum value of $p(t)$, δ is the extinction amplitude, and k is a pulse shaping parameter ranging from 1 to 2. Varying k from 1 to 2 results in rectangular to $\sin^2$ pulse shapes, respectively. The remaining (M-1) slots are represented by a constant power of δ^2.

For M-ary PPM systems, the ER is defined as the maximum optical power of the pulse to the average optical power of the remaining (M-1) slots. ER can be expressed in dB as:

$$\text{ER} = 10\log_{10}\left(\frac{P_{\max}}{\delta^2}\right) \text{dB}. \tag{4.14}$$

Figure 4.4 shows some examples of the lowpass equivalent electrical field of different pulse shapes (e.g., for $k = 1, 1.5,$ and 2) with finite and infinite extinction ratios.

The input field is amplified by the optical amplifier and also corrupted by the amplifier output noise, $n(t)$, which has two components. The polarization of the first component, denoted by $n_{\|}(t)$, is parallel to the input field polarization and the polarization of the sec-

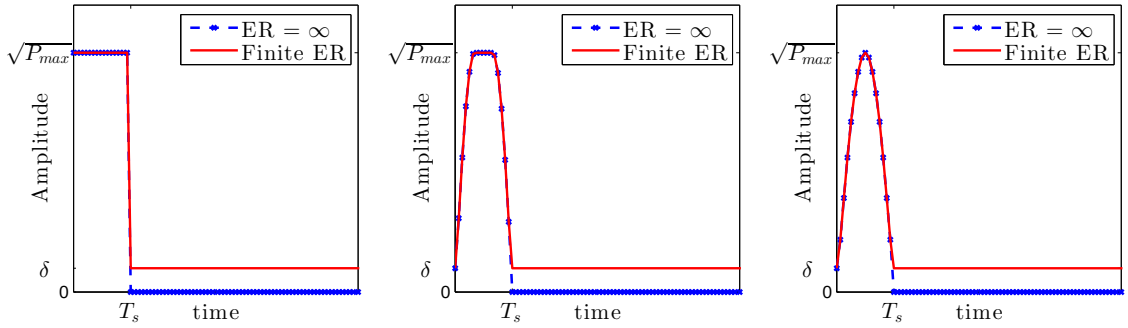

(a) $(k = 1)$ (b) $(k = 1.5)$ (c) $(k = 2)$

Figure 4.4: Lowpass Equivalent Electrical Field of M-ary PPM for Different Pulse Shapes.

ond component denoted by ,$n_\perp(t)$, is perpendicular to the input field polarization. Each of $n_\parallel(t)$ and $n_\perp(t)$ is modeled as a complex Gaussian noise process where the real and imaginary parts of this process have a zero mean and power spectral density N_{ASE} that is equal to $n_{sp}hf(G-1)$ which is also equal to $N_0(G-1)$, where N_0 is the single sided power spectral density of the amplifier equivalent input noise, G is the amplifier power gain, n_{sp} is the amplifier noise figure, h is Plank's constant, f is the optical frequency, and ASE is the amplifier spontaneous emission. The amplifier output field is given by:

$$E_{\text{out}}(t) = E_{\text{in}}(t)\sqrt{G} + n_\parallel(t) + n_\perp(t). \tag{4.15}$$

The amplifier output field is passed through the optical filter. The output of the optical filter is given by:

$$E_f(t) = \left(E_{\text{in}}(t)\sqrt{G} + n_\parallel(t)\right) * h(t) + n_\perp(t) * h(t). \tag{4.16}$$

The filter output is applied to a PIN photodiode to generate an electrical current I_{ph} that is given by:

$$I_{ph}(t) = \left|\left(E_{in}(t)\sqrt{G} + n_\parallel(t)\right) * h(t)\right|^2 + \left|n_\perp(t) * h(t)\right|^2, \tag{4.17}$$

where $h(t)$ is the impulse response of the optical filter and the "$*$" denotes linear convolution in the time domain. Then, the electrical current is directly applied to an electrical filter. The output of the electrical filter $v(t)$ is connected to an ideal electrical PPM receiver

where the BER is calculated. $v(t)$ is given by:

$$v(t) = I_{\text{ph}}(t) * h_{\text{elec}}(t), \tag{4.18}$$

where $h_{\text{elec}}(t)$ is the impulse response of the receiver electrical filter which is modeled as a third order butterworth filter. This electrical filter is practical for optical receivers [80, 81]. The electrical M-ary PPM receiver compares equally-spaced M samples taken from each symbol and decides on the transmitted r bits by taking the position of the maximum output.

4.3 Optically Preamplified 16-ary and 64-ary PPM Simulation Results

4.3.1 Optical Matched-Filters Results

To validate the simulation model for the 16-ary and 64-ary PPM systems, the cases where optical matched-filters are used were simulated. The optical matched-filters have a rectangular impulse response with a width equal to the slot time of the corresponding M-ary PPM system. As represented in Figure 4.5, the results for 16-ary and 64-ary PPM systems affected only by $n_{\|}$ agree with the closed form expression in Equation 4.8.

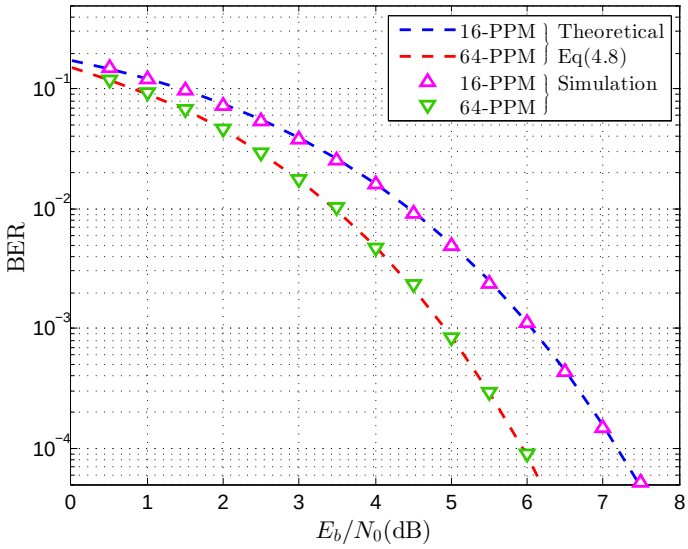

Figure 4.5: Theoretical and Simulation BER Results for Optically Preamplified 16-ary and 64-ary PPM Systems Using Optical Matched-Filters (1 ASE).

Figure 4.6 shows that the simulation results for the systems affected by $n_{\parallel}$ and $n_{\perp}$ agree with the theoretical expression provided by Equation 4.11.

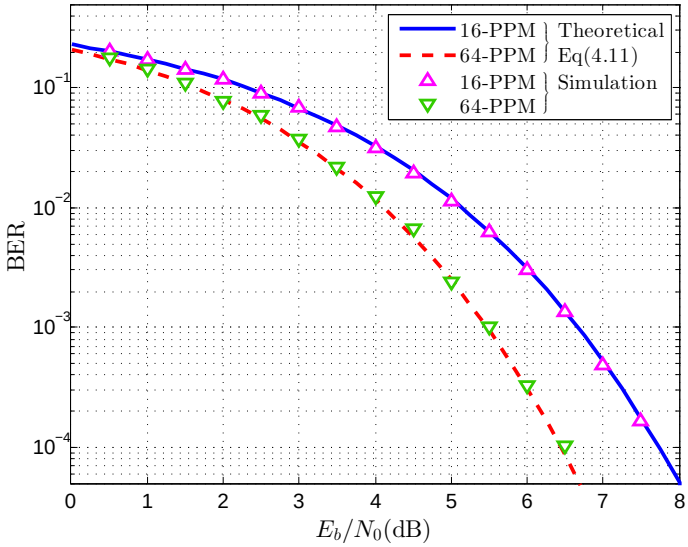

Figure 4.6: Theoretical and Simulation BER Results for Optically Preamplified 16-ary and 64-ary PPM Systems Using Optical Matched-Filters (2 ASE).

4.3.2 Optical and Electrical Filters Bandwidths Optimization

To evaluate the performance of practical 16-ary and 64-ary PPM systems, the optical matched-filter was replaced with a Fabry Pérot filter and an electrical filter was considered after the photodiode. The Fabry Pérot filter was modeled as a first order low pass filter and the electrical filter as a third order butterworth filter. In this evaluation, $n_{\parallel}$ and $n_{\perp}$ were considered and the thermal noise was ignored as it was assumed to be much smaller than $n_{\parallel}$ and $n_{\perp}$.

There is a joint optimal selection of the optical and electrical filter bandwidths which provides the minimum E_b/N_0 performance penalty relative to the matched-filter performance. This optimality is a trade-off between the noise-filtering and the signal-filtering effects. Increasing the BW of the optical filter will reduce the rejection of the signal-independent noise (ASE-ASE noise) and hence degrades the performance. On the other hand, decreasing the BW of the optical filter increases the ASE-ASE noise rejection. Further BW reduction causes filtering to some contents of the desired signal and hence degrades the performance. The electrical filter's role is to reduce the ASE-ASE noise as well

as the ASE-signal noise components. As for the optical filter, increasing or decreasing the BW of the electrical filter is a trade-off between noise filtering and signal filtering [16].

In this study, four systems were mainly addressed. Those are the 16-ary PPM systems with a rectangular pulse ($k = 1$) and with a $\sin^2$ pulse ($k = 2$), and the 64-ary PPM systems with a rectangular pulse and with a $\sin^2$ pulse. In order to optimize the optical/electrical pair in each of the studied systems, the bandwidths of the optical and the electrical filters were varied in steps of 8% and 1.8% of the slot rate (R_s), respectively. In M-ary PPM, R_s is related to the bit rate R_b as follows:

$$R_s = \frac{M}{\log_2 M} R_b. \tag{4.19}$$

The range of the FWHM of the Fabry Pérot filter was taken from $0.25R_s$ to $4.5R_s$ and for the 3-dB bandwidth of the electrical filter was taken from $0.5R_s$ to $4R_s$. For the penalty calculations, a mesh of the electrical and optical bandwidths was used where the penalty from the matched-filter results at 10^{-3} was evaluated for each pair. The penalty was calculated relative to 6.7 dB for the 16-ary PPM systems and to 5.5 dB for the 64-ary PPM systems. These values represent the E_b/N_0 performances at 10^{-3} for systems using an optical matched-filter and affected by $n_{\|}$ and $n_{\perp}$.

Figure 4.7 represents the contour results for the performance penalty as a function of the FWHM of the Fabry Pérot filter and the 3-dB bandwidth of the electrical filter both normalized by the bit rate. For 16-ary PPM systems where $k = 1$, an optimum combination of a FWHM of $3.2R_b$ for the Fabry Pérot filter and a 3 dB-bandwidth of $3R_b$ for the electrical filter was selected. This pair causes around 0.6 dB penalty as seen in Figure 4.7(a). For 16-ary PPM systems with $k = 2$, an optimum combination of a FWHM of $4R_b$ for the Fabry Pérot filter and a 3 dB-bandwidth of $4R_b$ for the electrical filter results in a penalty of 0.2 dB as shown in Figure 4.7(b). An optimum combination for the 64-ary PPM systems with $k = 1$ was selected to be a FWHM of $7.5R_b$ for the Fabry Pérot filter and a 3 dB-bandwidth of $8R_b$ for the electrical filter. A minimal penalty of 0.7 dB was obtained as shown in Figure 4.7(c). For the 64-ary PPM systems with $k = 2$, an optimum

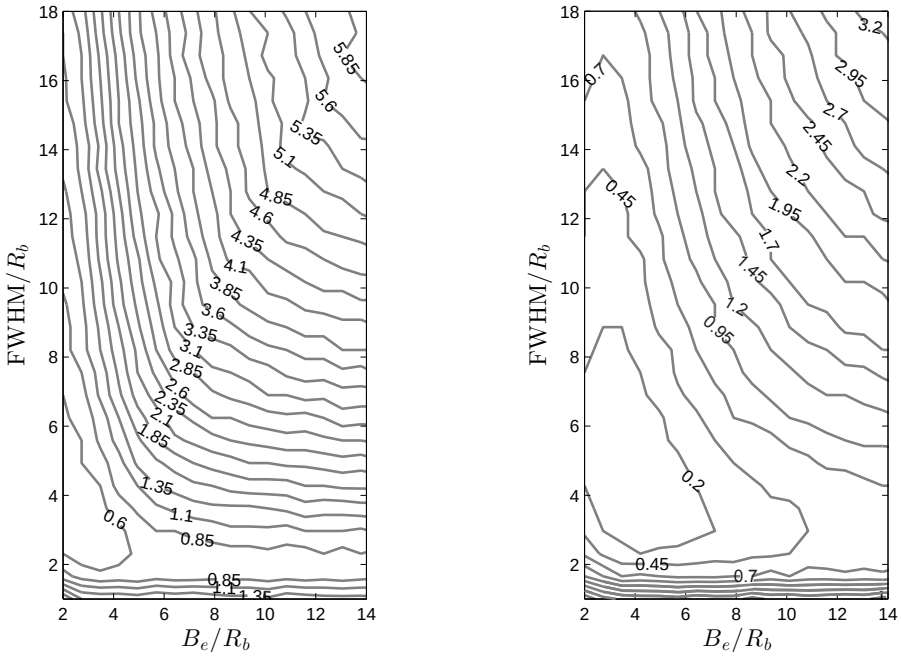

(a) 16-ary PPM Systems ($k = 1$)

(b) 16-ary PPM Systems ($k = 2$)

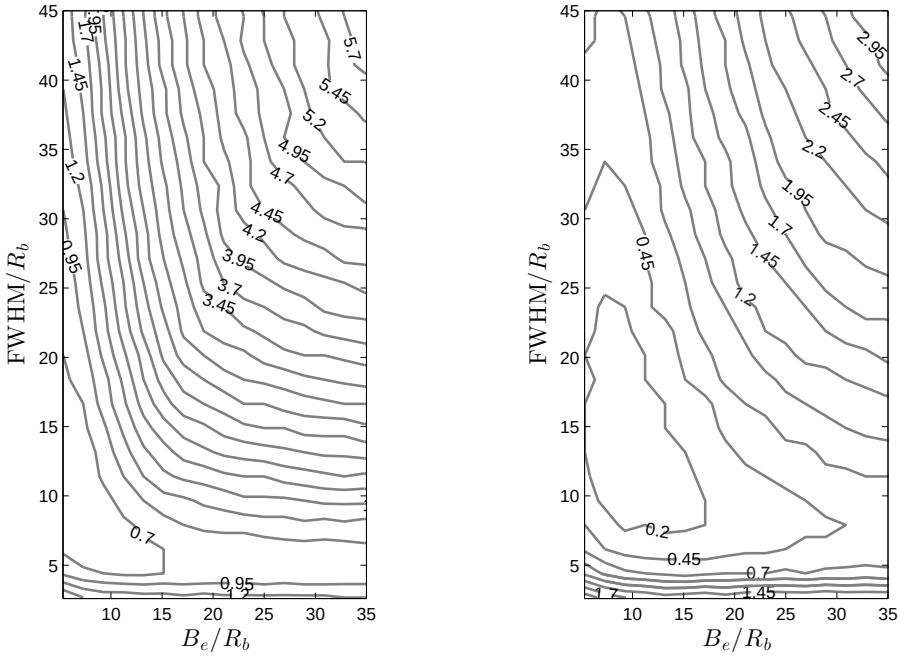

(c) 64-ary PPM Systems ($k = 1$)

(d) 64-ary PPM Systems ($k = 2$)

Figure 4.7: Performance Penalty as a Function of the FWHM of the Fabry-Pérot Filter and the 3-dB Bandwidth of the Electrical Filter (B_e) both Normalized to the Bit Rate (R_b).

combination of a FWHM of $15R_b$ for the Fabry Pérot filter and a 3 dB-bandwidth of $10R_b$ for the electrical filter was selected. This caused a penalty of 0.2 dB as can be seen from Figure 4.7(d).

4.3.3 BER Results

After optimizing the optical and electrical filters in optically preamplified 16-ary and 64-ary PPM systems, the effect of finite extinction ratios on the BER performance was studied. Finite ER breaks the orthogonality in M-ary PPM systems and thus results in performance degradations when compared to the ideal case of infinite ER. The BER results for the 16-ary and the 64-ary PPM systems with $k = 1$ and $k = 2$ were generated at infinite and finite ERs. For the case of finite ER, simulations were carried for ER values of 25, 20, and 15 dB. For the infinite and finite ER cases, $n_{\|}$ and $n_{\perp}$ were considered and the optimum combination of optical and electrical filters was used. Figure 4.8 represents the 16-ary PPM systems with $k = 1$, where an optimum combination of a FWHM of $3.2R_b$ for the Fabry Pèrot Filter and a 3 dB-BW of $3R_b$ for the electrical filter was used. The theoretical results for the 16-ary PPM systems using matched filters (MF) were also included to evaluate the performance penalties. Under 20 dB ER, the required E_b/N_0 to achieve a BER of 10^{-3} is approximately 8 dB.

Figure 4.9 represents the BER results for the 16-ary PPM systems with $k = 2$, where an optimum combination of a FWHM of $4R_b$ for the Fabry Pérot filter and a 3 dB-BW of 4 R_b for the electrical filter was used. Under 20 dB ER, the required E_b/N_0 to achieve a BER of 10^{-3} is approximately 8.2 dB. Figures 4.10 and 4.11 show the BER results for the 64-ary PPM systems with $k = 1$ and 2, respectively. The optimum combination of the optical and electrical filters was used in each case. Under 20 dB ER, the performance at 10^{-3} is 8.35 dB for systems with $k = 1$ and 9.6 dB for systems with $k = 2$. Tables 4.1, 4.2, 4.3, and 4.4 summarize the required E_b/N_0 to achieve a target BER of 10^{-3} and also provide the corresponding PPB when n_{sp}=1 and 3. From Table 2.1, optically preamplified 16-ary PPM systems with $k = 1$ and 2 ASE can establish 10 Gbps inter-satellite links using a practical value of $n_{sp} = 3$ and an optical antenna diameter of 0.16 m.

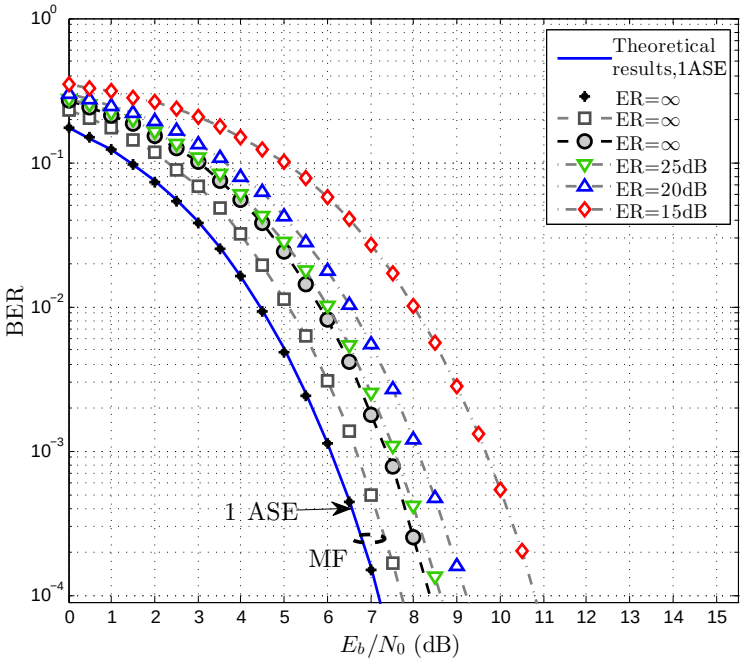

Figure 4.8: BER Results for Optically Preamplified 16-PPM Systems with $k = 1$ (Fabry Pérot Filter FWHM = $3.2R_b$, Electrical Filter 3 dB-BW = 3 R_b).

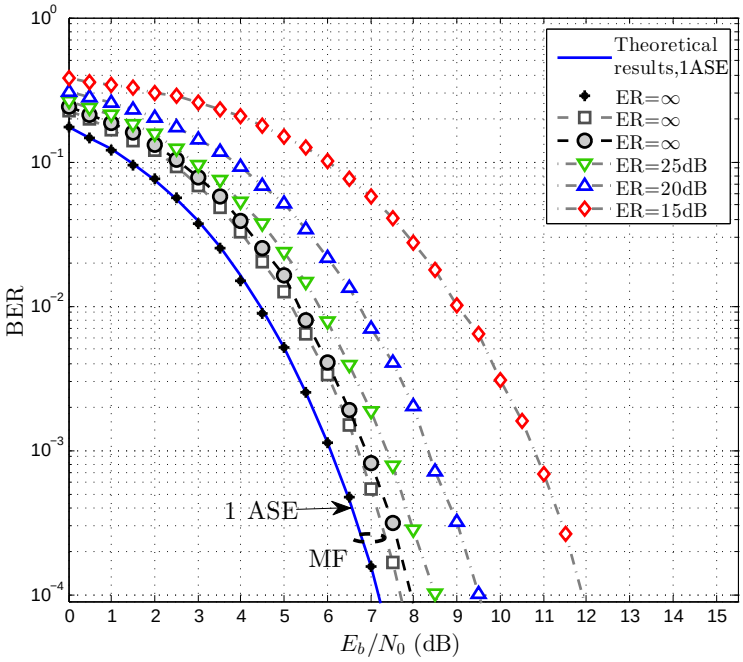

Figure 4.9: BER Results for Optically Preamplified 16-PPM Systems with $k = 2$ (Fabry Pérot Filter FWHM = $4R_b$, Electrical Filter 3 dB-BW = 4 R_b).

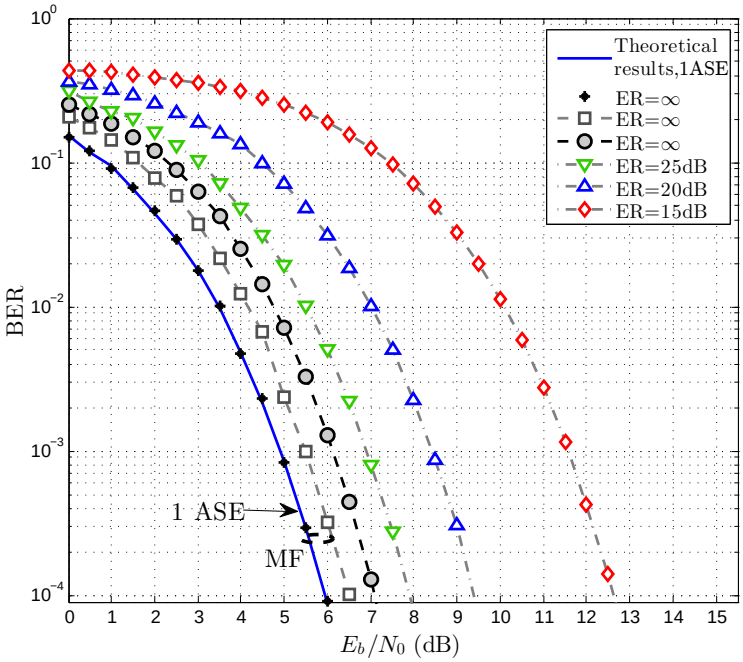

Figure 4.10: BER Results for Optically Preamplified 64-PPM Systems with $k = 1$ (Fabry Pérot Filter FWHM = 7.5R_b, Electrical Filter 3 dB-BW = 8 R_b).

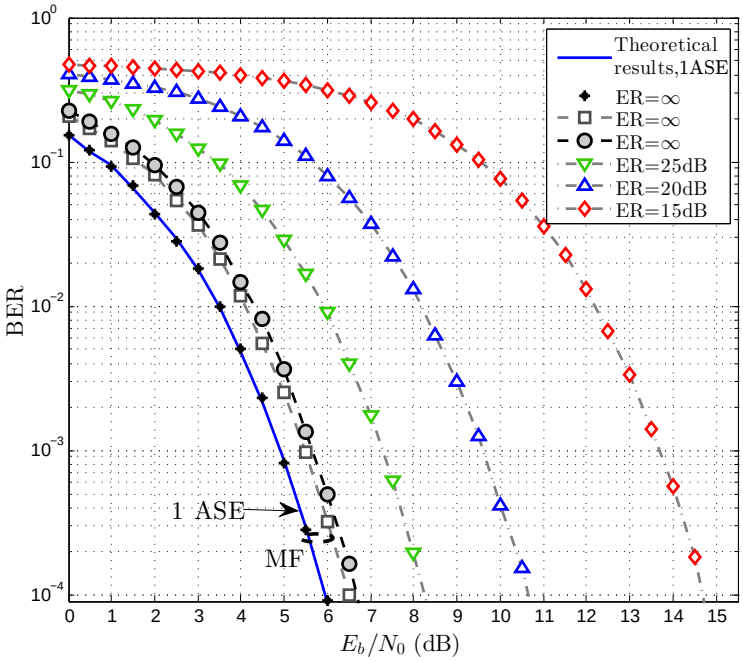

Figure 4.11: BER Results for Optically Preamplified 64-PPM Systems with $k = 2$ (Fabry Pérot Filter FWHM = 15R_b, Electrical Filter 3 dB-BW = 10 R_b).

Table 4.1: Performance of Optically Preamplified 16-ary PPM Systems at BER of 10^{-3} for k=1

	MF 1 ASE ER = ∞	MF 2 ASE ER = ∞	FP and EF$*$ 2 ASE ER = ∞	FP and EF$*$ 2 ASE ER = 25 dB	FP and EF$*$ 2 ASE ER = 20 dB	FP and EF$*$ 2 ASE ER = 15 dB
E_b/N_0 (dB)	6	6.7	7.35	7.43	8	9.55
PPB ($n_{sp} = 1$)	4	4.7	5.4	5.5	6.3	9
PPB ($n_{sp} = 3$)	12	14.1	16.2	16.5	18.9	27

$*$ Optimum combination of FWHM of $3.2R_b$ for the Fabry Pérot filter and 3 dB-BW of 3 R_b for the electrical filter

Table 4.2: Performance of Optically Preamplified 16-ary PPM Systems at BER of 10^{-3} for k=2.

	MF 1 ASE ER = ∞	MF 2 ASE ER = ∞	FP and EF$\star$ 2 ASE ER = ∞	FP and EF$\star$ 2 ASE ER = 25 dB	FP and EF$\star$ 2 ASE ER = 20 dB	FP and EF$\star$ 2 ASE ER = 15 dB
E_b/N_0 (dB)	6	6.7	6.9	7.25	8.2	10.65
PPB ($n_{sp} = 1$)	4	4.7	5	5.3	6.6	11.6
PPB ($n_{sp} = 3$)	12	14.1	15	15.9	19.8	34.8

$\star$ Optimum combination of FWHM of $4R_b$ for the Fabry Pérot filter and 3 dB-BW of 4 R_b for the electrical filter

Table 4.3: Performance of Optically Preamplified 64-ary PPM Systems at BER of 10^{-3} for k=1.

	MF 1 ASE ER = ∞	MF 2 ASE ER = ∞	FP and EF‡ 2 ASE ER = ∞	FP and EF‡ 2 ASE ER = 25 dB	FP and EF‡ 2 ASE ER = 20 dB	FP and EF‡ 2 ASE ER = 15 dB
E_b/N_0 (dB)	4.9	5.5	6.1	6.85	8.35	11.5
PPB ($n_{sp} = 1$)	3.1	3.5	4.1	4.8	6.8	14.1
PPB ($n_{sp} = 3$)	9.3	10.5	12.3	14.4	20.4	42.3

‡ Optimum combination of FWHM of $7.5R_b$ for the Fabry Pérot filter and 3 dB-bandwidth of 8 R_b for the electrical filter

Table 4.4: Performance of Optically Preamplified 64-ary PPM Systems at BER of 10^{-3} for k=2.

	MF 1 ASE ER = ∞	MF 2 ASE ER = ∞	FP and EF§ 2 ASE ER = ∞	FP and EF§ 2 ASE ER = 25 dB	FP and EF§ 2 ASE ER = 20 dB	FP and EF§ 2 ASE ER = 15 dB
E_b/N_0 (dB)	4.9	5.5	5.65	7.18	9.6	13.6
PPB ($n_{sp} = 1$)	3.1	3.5	3.7	5.2	9.12	22.9
PPB ($n_{sp} = 3$)	9.3	10.5	11.1	15.6	27.36	68.7

§ Optimum combination of FWHM of $15R_b$ for the Fabry Pérot filter and 3 dB-bandwidth of 10 R_b for the electrical filter

4.3.4 Finite Extinction Ratio Results

The performance penalties due to ERs ranging from 35 dB to 15 dB were evaluated. The E_b/N_0 penalties at 10^{-3} for the four cases addressed are shown in Figure 4.12. The E_b/N_0 penalties for the cases of the 16-ary and the 64-ary PPM systems were evaluated relative to 6.7 dB and 5.5 dB, respectively. These values represent the E_b/N_0 values required to obtain a BER of 10^{-3} for the systems affected by $n_{\|}$ and $n_{\perp}$ and use optical matched-filters under no extinction ratio.

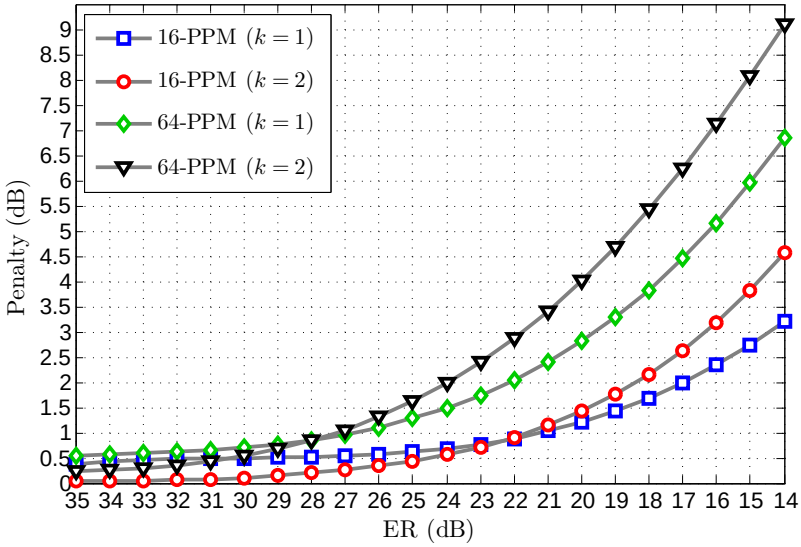

Figure 4.12: Penalty Due to Finite Extinction Ratio.

For each case, the optimum pair of the FWHM of the optical filter and the 3-dB BW of the electrical filter was used. Results at a high value of ER such as 35 dB are around 0.2 dB for the $\sin^2$ pulse shape and around 0.6 dB for the rectangular pulse shape. These results represent the penalties due to replacing the matched-filter with the optimum optical and electrical filters pair. At an ER of 20 dB, the penalties for the 16-ary PPM systems are 1.3 dB when $k = 1$ and 1.5 dB when $k = 2$, resulting in E_b/N_0 performances of 6.7 + 1.3 = 8 dB and 8.2 dB, respectively. For the 64-ary PPM systems at an ER of 20 dB, the E_b/N_0 penalties are 2.85 dB when $k = 1$ and 4.1 dB when $k = 2$, resulting an E_b/N_0 performances of 8.35 dB and 9.6 dB, respectively.

In the ideal case (i.e., when the ER is infinite), the 64-ary PPM systems perform better than the 16-ary PPM systems. However, it can be noticed from Figure 4.12 and the results discussed above that decreasing the ER value results in penalty increase as M increases. As a result, the 16-ary PPM systems outperform the 64-ary PPM systems at low ER values. Also, as the ER decreases, the penalties for the systems with $k = 2$ are higher than the penalties for systems with $k = 1$ for the same value of M.

To justify these results, the orthogonality of M-ary PPM systems is examined under different values of the ER. In the ideal case of infinite ER, all symbols of the M-ary PPM signals are orthogonal. On the other hand, when the ER is finite, the symbols are correlated and the system is no longer orthogonal. To examine the effects of finite ER on M-ary PPM systems, the cross-correlation between two different symbols normalized by the power in the symbol was calculated. The normalized cross correlation between the electrical field of symbols s_0 and s_1 is expressed as:

$$\rho_{1,2} = \frac{\int_{t=0}^{T_{\text{sym}}} s_1(t)s_2(t)dt}{\int_{t=0}^{T_{\text{sym}}} s_1^2(t)dt},$$

where T_{sym} is the M-ary PPM symbol duration. Figure 4.13 represents the normalized cross-correlation coefficient ($\rho_{1,2}$) as a function of M for different ER values.

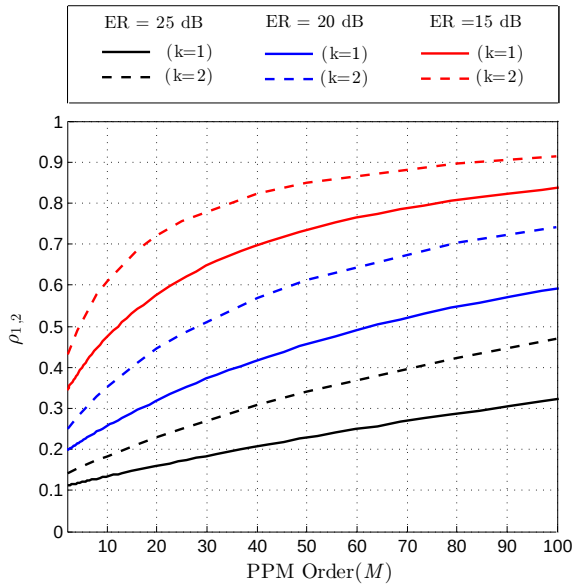

Figure 4.13: $\rho_{1,2}$ versus M for Different Extinction Ratios.

Higher values of $\rho_{1,2}$ indicate a higher correlation between the symbols and hence degraded performance for the M-ary PPM systems. For finite ER values, increasing M increases $\rho_{1,2}$. Also, $\rho_{1,2}$ for systems with $k = 2$ is higher than for systems with $k = 1$. These relations justify the penalty results represented in Figure 4.12. In Figure 4.12, the penalties for the systems with $k = 2$ are higher than the systems with $k = 1$. Also, as the ER decreases, the penalties for the 64-ary PPM systems compared to the penalties for the 16-ary PPM systems increase at a higher rate.

4.3.5 Non-Ideal Receivers Results

For systems using the optimum combination of the optical and electrical filters at an ER value of 20 dB, the degradations due to the non-ideal characteristics in the optical receivers are evaluated. At the electrical detection circuitry, variations in the position of the decision sample from the optimum position usually lead to degraded BER performance. The movement of the optical transceivers in FSO links causes frequency drifts in the transmitted optical signal due to Doppler effects. In this case, the optical carrier frequency of the incoming optical signal is no longer centered at the optical and electrical bandpass filters and the performance of the system will degrade. In the following subsection, the penalties due to timing jitter and frequency drifts up to $2R_b$ Hz are evaluated.

(a) Timing Jitter

Figure 4.14 depicts the performance penalty due to timing jitter at the decision circuitry. The range for the jitter (Δt) in this evaluation is $\pm 25\%$ of the slot time T_s, where $T_s = 1/R_s$ and R_s is the slot rate. Penalty results were calculated in steps of $1/(16 \times R_s)$. The penalties were evaluated relative to the systems affected by $n_{\|}$ and $n_{\perp}$ and using the optimum combination of the electrical and the optical filters under 20 dB ER with optimum sampling. Those penalties are 8, 8.2, 8.35, and 9.6 dB for the 16-ary PPM systems with $k = 1$ and $k = 2$ and for the 64-ary PPM systems with $k = 1$ and $k = 2$, respectively. It is worth mentioning that the optimum sampling point is at the higher expected amplitude of the electrical filter output.

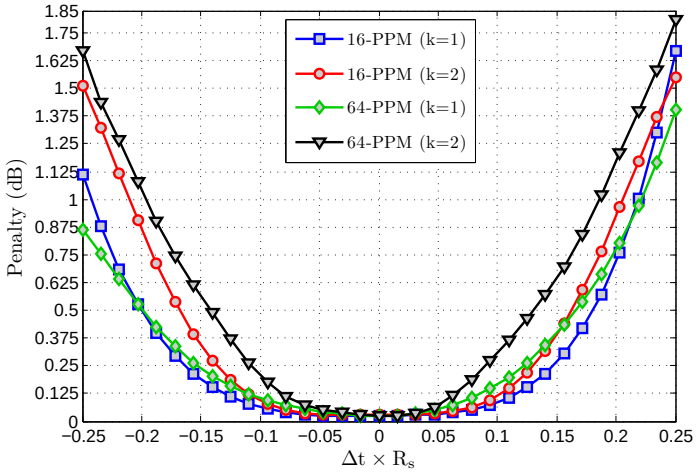

Figure 4.14: Sensitivity Penalty Due to Deterministic Electronic Jitter.

As expected, the penalties for the 16-ary and the 64-ary PPM systems with $k = 2$ (rounded pulses) are higher than the penalties for the systems with $k = 1$ (rectangular pulses). This is because the amplitude of the electrical filter output decays faster in the case of the $\sin^2$ pulses than the case of rectangular pulses. The maximum penalty due to deterministic jitter is around 1.75 dB for 64-ary PPM systems with $k = 2$.

(b) Frequency Drift

Figure 4.15 shows the penalty due to frequency drifts up to $2R_b$ Hz. The bit rate was assumed to be 10 Gbps; thus the evaluation is up to a frequency drift of 20 GHz. The penalty was evaluated relative to the systems affected by $n_{\parallel}$ and $n_{\perp}$ and using the optimum combination of the electrical and the optical filters under 20 dB ER without frequency drift. As in the jitter penalty evaluation, those penalties are 8, 8.2, 8.35, and 9.6 dB for the 16-ary PPM systems with $k = 1$ and $k = 2$, and for the 64-ary PPM systems with $k = 1$ and $k = 2$, respectively.

As can be seen from Figure 4.15, the penalty due to a frequency drift of 10 GHz can be neglected for 64-ary PPM systems and for 16-ary PPM systems with $k = 2$. For a 16-ary PPM system with $k = 1$, the penalty is approximately 0.2 dB. At a frequency drift of 20 GHz, the penalties are 1.4 dB and 0.6 dB for 16-ary PPM with $k = 1$ and $k = 2$,

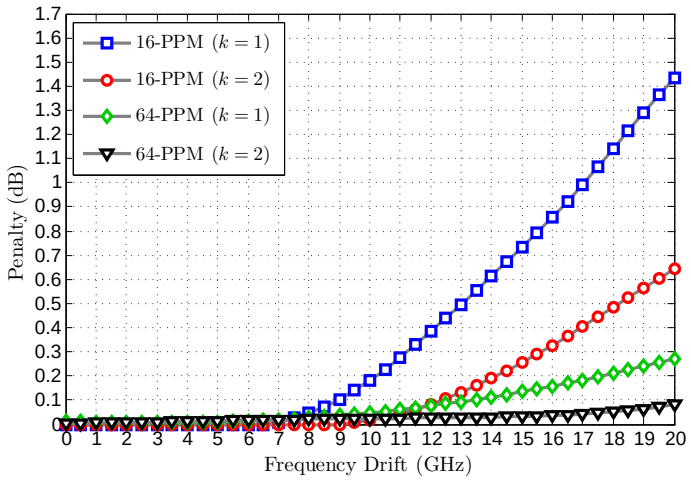

Figure 4.15: Sensitivity Penalty Due to Frequency Drift.

respectively. For 64-ary PPM systems, the penalties are 0.25 dB and 0.1 dB, respectively. The difference in the penalties can be justified by the differences in the bandwidths of the optimum optical and electrical filters in each case. As the bandwidth of the filters increases, the ability of tolerating frequency drifts increases.

Chapter 5

Performance Evaluation of PDM-BPSK and PDM-QPSK M-ary PPM Modulation Schemes

M-ary PPM combined with polarization division multiplexed-Quadrature phase shift keying (PDM-QPSK M-ary PPM) was recently introduced and demonstrated in order to achieve higher sensitivity than conventional M-ary PPM systems. This chapter starts by introducing PDM-QPSK and PDM-binary phase shift keying (PDM-BPSK) modulation schemes. Then, the performance of PDM-BPSK M-ary PPM and PDM-QPSK M-ary PPM is examined. Finally, the penalties due to finite extinction ratio for $M \in [8, 16, 64]$ are presented.

5.1 PDM-BPSK and PDM-QPSK Modulation Schemes

PDM-BPSK and PDM-QPSK modulation schemes were introduced in Chapter 2. In these modulation formats, both the polarization and phase shift of the optical field are used to encode the data. In the following subsections, theoretical BER performances of PDM-BPSK and PDM-QPSK modulation schemes are discussed.

5.1.1 PDM-BPSK

The BER performance of the BPSK modulation scheme can be found in [71] and is expressed as:

$$\text{BER}_{\text{BPSK}} = 0.5 \text{ erfc}\left(\sqrt{E_s/N_0}\right), \tag{5.1}$$

where erfc is the error function and $E_s/N_0 = E_b/N_0$. Then, the BER performance of PDM-BPSK can be given as:

$$\text{BER}_{\text{PDM - BPSK}} = 0.5 \text{ erfc}\left(\sqrt{E_s/N_0/2}\right), \tag{5.2}$$

where $E_s/N_0 = 2 \times E_b/N_0$. PDM-BPSK has the same performance as BPSK because the transmitted power is doubled and the BPSK signals in each polarization are orthogonal. Figure 5.1 shows the system model of an optically preamplified PDM-BPSK. An example of the lowpass equivalent of the PDM-BPSK signal in both polarizations is shown. The optical preamplifier adds two ASE noise sources; however, for perfect phase/polarization diversity systems, the Q component of the noise in the x polarization and the Q component of the noise in the y polarization are eliminated. Thus, the performance of optically preamplified PDM-BPSK systems follows Equation 5.2.

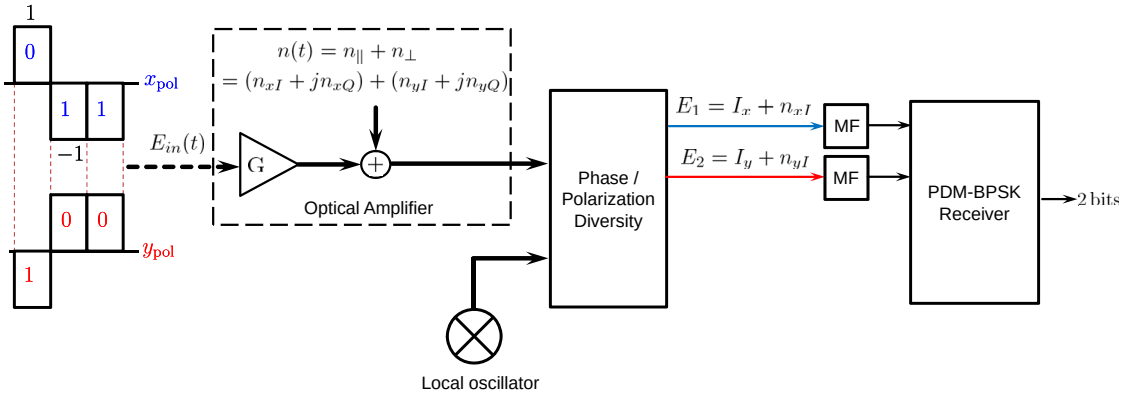

Figure 5.1: Optically Preamplified PDM-BPSK System Model.

5.1.2 PDM-QPSK

The BER performance of QPSK modulation format can be found in [71] and is expressed as:

$$\text{BER}_{\text{QPSK}} = 0.5 \text{ erfc}\left(\sqrt{E_s/N_0/2}\right), \tag{5.3}$$

where $E_s/N_0 = 2 \times E_b/N_0$. The BER performance of PDM QPSK can be found in [57,

58, 59, 24] and is given as:

$$\text{BER}_{\text{PDM - QPSK}} = 0.5 \text{ erfc}\left(\sqrt{E_s/N_0/4}\right), \tag{5.4}$$

where $E_s/N_0 = 4 \times E_b/N_0$. PDM-QPSK has the same performance as QPSK as well as BPSK because the transmitted power is multiplied by four and the I and Q components of the QPSK signals are orthogonal. Also, the QPSK signals in each polarization are orthogonal. Figure 5.2 shows the system model of an optically preamplified PDM-QPSK. An example of the I and Q components of the PDM-QPSK signal in both polarizations is shown. For a perfect phase/polarization diversity system, the I and the Q components of the noise in the x polarization will be added to the I and the Q signal components in the x polarization. Similarly, the I and the Q component of the noise in the y polarization will be added to the I and the Q signal components in the y polarization. Thus, the performance of optically preamplified PDM-QPSK systems follows Equation 5.4.

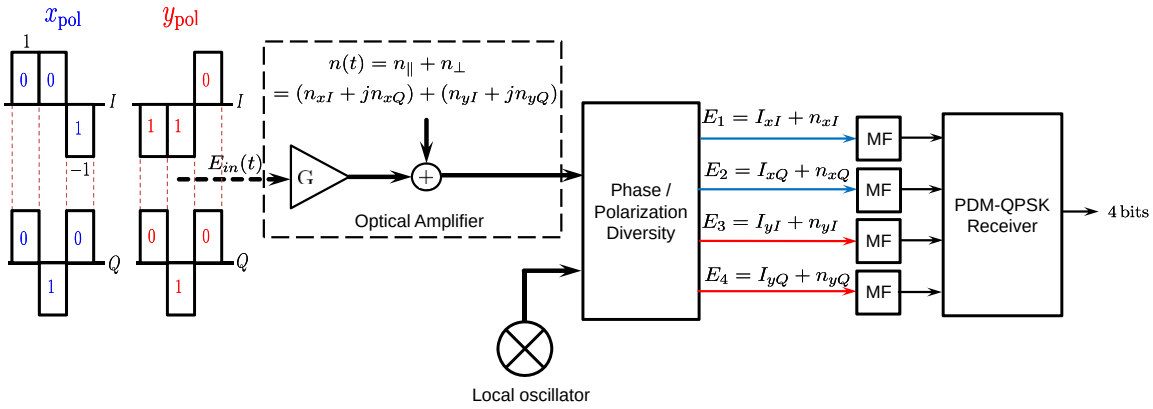

Figure 5.2: Optically Preamplified PDM-QPSK System Model.

5.2 PDM-BPSK and PDM-QPSK M-ary PPM Modulation Schemes

In PDM-BPSK and PDM-QPSK M-ary modulation schemes, the polarization, phase shift, and location of the optical pulse are used to encode the data. In the following subsections, theoretical BER performances of PDM-BPSK and PDM-QPSK M-ary modulation schemes are discussed.

5.2.1 PDM-BPSK-M-ary PPM

The system model of PDM-BPSK M-ary PPM is shown in Figure 5.3. An example of the lowpass equivalent signal is also shown. The sum of the magnitude square of the matched-filter (MF) outputs are used to identify the pulse location. Then, the PDM-BPSK bits are determined at that location from the MF output. Symbol errors in PDM-BPSK-M-ary PPM symbols have two causes. When the M-ary PPM slot is identified incorrectly, an average of $\frac{M}{2(M-1)}\log_2(M)$ of the $r = \log_2(M)$ bits, corresponding to the M-ary PPM, is in error. This is in addition to an average of $\frac{0+1+2}{3} = 1$ bits in error, corresponding to the PDM-BPSK. The other cause of symbol errors is when the M-ary PPM slot is identified correctly, but the bits corresponding to the PDM-BPSK are in error. In this case, the BER of PDM-BPSK M-ary PPM systems (PB-M-ary PPM) will be:

$$\text{BER}_{\text{PB-M-PPM}} = \frac{\text{SER}_{\text{M - PPM}}\left[1 + \frac{M\log_2 M}{2(M-1)}\right] + (1 - \text{SER}_{\text{M - PPM}})\left[2\text{BER}_{\text{PDM - BPSK}}\right]}{\log_2 M + 2}, \quad (5.5)$$

where $\text{SER}_{\text{M - PPM}}$ is the SER of the M-ary PPM systems with one ASE noise source and is given by Equation 4.6 and $\text{BER}_{\text{PDM - BPSK}}$ is given by Equation 5.2.

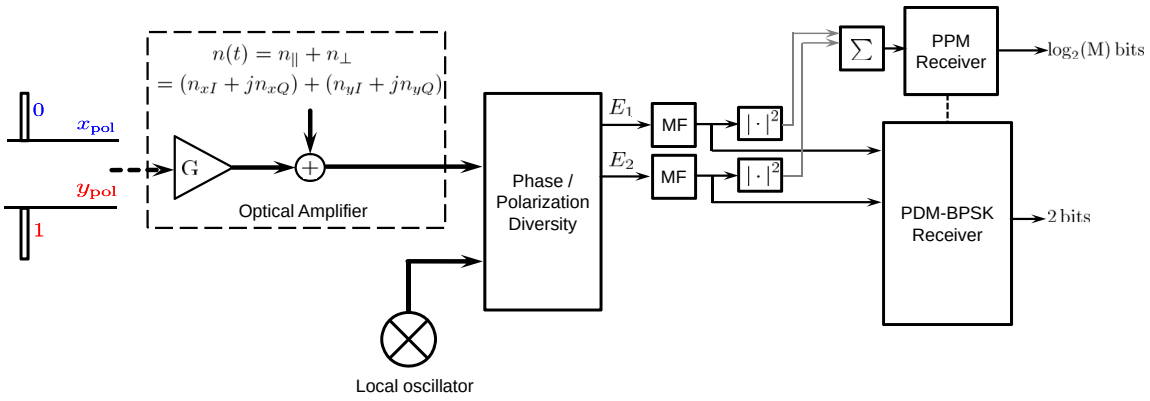

Figure 5.3: Optically Preamplified PDM-BPSK M-ary PPM System Model.

5.2.2 PDM-QPSK-M-ary PPM

Figure 5.4 shows the system model for PDM-QPSK M-ary PPM and shows an example of the lowpass equivalent signal. The detection in PDM-QPSK M-ary PPM systems is similar to the detection in PDM-BPSK systems with the difference being that four bits are identified by the PDM-QPSK demodulator. Symbol errors in PDM-QPSK-M-ary PPM have two causes. When the M-ary PPM slot is identified incorrectly, an average of $\frac{M}{2(M-1)}\log_2(M)$ of the $r = \log_2(M)$ bits, corresponding to the M-ary PPM, is in error. Also an average of $\frac{0+1+2+3+4}{5} = 2$ bits is in error, corresponding to the PDM-QPSK. The other symbol errors cause is when the M-ary PPM slot is correctly identified, but the bits corresponding to the PDM-QPSK are in error. In this case, the BER of PDM-QPSK M-ary PPM systems (PQ-M-ary PPM) will be [24]:

$$\text{BER}_{\text{PQ -M-PPM}} = \frac{\text{SER}_{\text{M - PPM}}\left[2 + \frac{M\log_2 M}{2(M-1)}\right] + (1 - \text{SER}_{\text{M - PPM}})\left[4\text{BER}_{\text{PDM - QPSK}}\right]}{\log_2 M + 4}, \quad (5.6)$$

where $\text{SER}_{\text{M - PPM}}$ corresponds to the SER of the M-ary PPM systems with two ASE noise sources and is given by Equation 4.11 and $\text{BER}_{\text{PDM - QPSK}}$ is given by Equation 5.4.

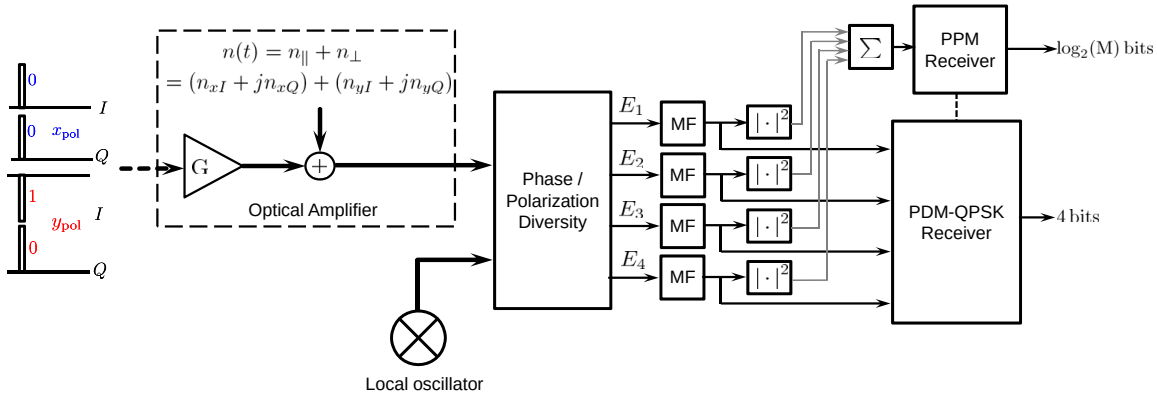

Figure 5.4: Optically Preamplified PDM-QPSK M-ary PPM System Model.

5.3 Optically Preamplified PDM-QPSK and PDM-BPSK M-ary PPM Receivers Simulation Models

5.3.1 PDM-BPSK M-ary PPM

Figure 5.5 represents the simulation model used to evaluate the BER performance of PDM-BPSK M-ary PPM systems. White Gaussian noise is added to each signal component. This is equivalent to the operation of a perfect phase/polarization diversity block, where the noise and the signal components in the x and the y polarization are perfectly separated. Each of those electrical signals is then passed to a matched-filter and the magnitude square for each is evaluated. The sum of the magnitude squares is used to identify the M-ary PPM slot and the corresponding $\log_2(M)$ bits. The location of the slot is used to identify the two PDM-QPSK bits from the output of the matched-filter. The BER is then evaluated.

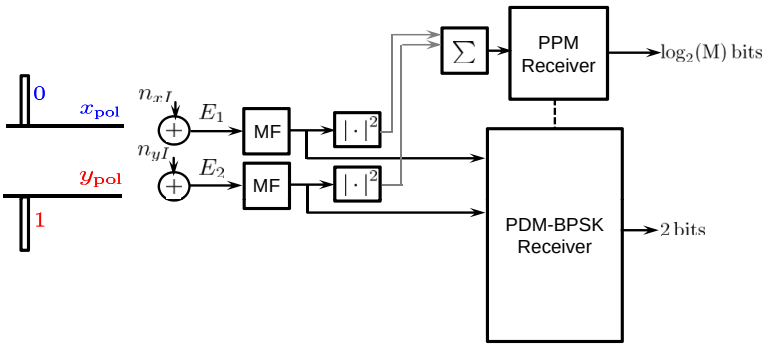

Figure 5.5: Optically Preamplified PDM-BPSK M-ary PPM Simulation Model.

5.3.2 PDM-QPSK M-ary PPM

Figure 5.6 represents the simulation model used to evaluate the BER performance of PDM-QPSK M-ary PPM systems. White Gaussian noise is added to each signal component. This is equivalent to the operation of a perfect phase/polarization diversity block, where, the I and Q components in the x and the y polarization are perfectly separated. Each of those electrical signals is then passed to a matched-filter and the magnitude square

for each is evaluated. The sum of the magnitude squares is used to identify the M-ary PPM slot and the corresponding $\log_2(M)$ bits. The location of the slot is used to identify the four PDM-QPSK bits from the output of the matched filter. The BER is then evaluated.

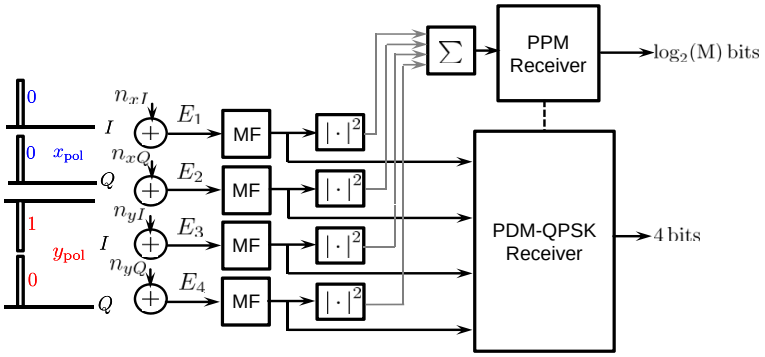

Figure 5.6: Optically Preamplified PDM-QPSK M-ary PPM Simulation Model.

5.4 Simulation Results

(a) Simulation Results for PDM-BPSK M-ary PPM

Figure 5.7 represents the BER results for the PDM-BPSK M-ary PPM (PB-M-ary PPM) systems. Equation 5.5 was used to obtain the theoretical performance for $M \in [4, 8, 16, 32, 64]$. Simulation results for the same values of M using the simulation model described in subsection (5.3.1) are identical to the theoretical results.

(b) Simulation Results for PDM-QPSK M-ary PPM

Figure 5.8 shows the BER results for the PDM-QPSK M-ary PPM (PQ-M-ary PPM) systems. Equation 5.6 was used to obtain the theoretical performance for $M \in [4, 8, 16, 32, 64]$. Simulation results for the same values of M using the simulation model described in subsection (5.3.2) are also identical to the theoretical results.

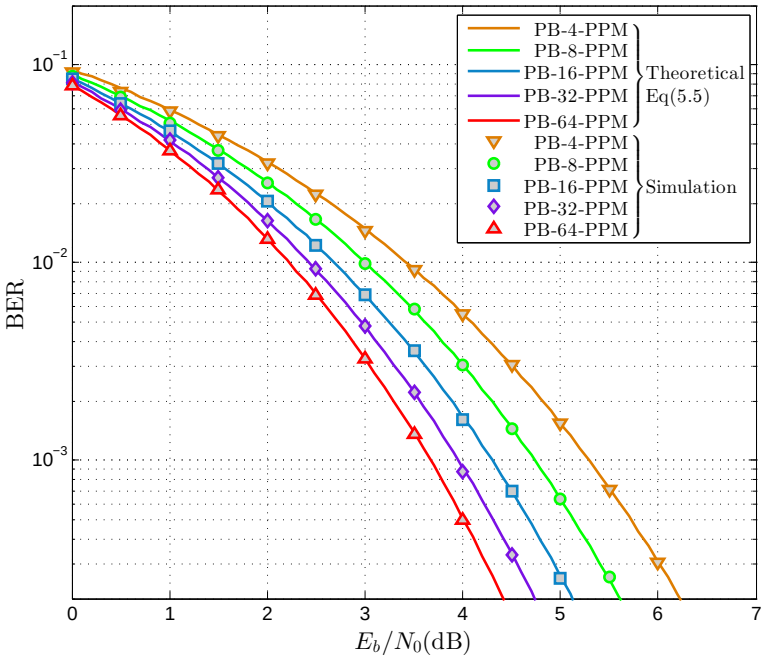

Figure 5.7: PDM-BPSK M-ary PPM Theoretical and Simulation Results.

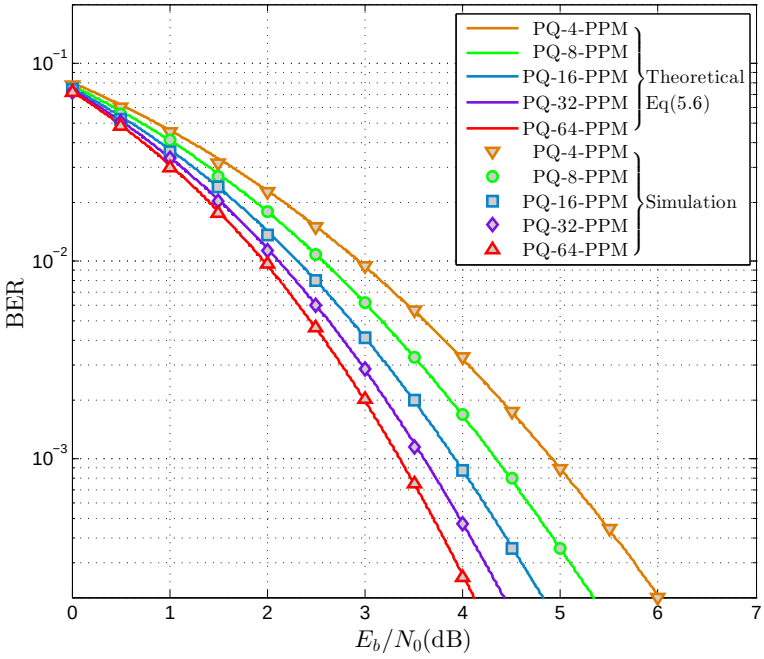

Figure 5.8: PDM-QPSK M-ary PPM Theoretical and Simulation Results.

Tables 5.1 and 5.2 summarize the E_b/N_0 as well as the PPB for $n_{sp} = 1$ and 3 values required to obtain a BER of 10^{-3}. The results in Table 5.2 match the results presented in [57, 58, 59, 24]. Table 5.3 is obtained from Figure 4.2 and is provided here to be compared to PDM-BPSK and PDM-QPSK M-ary PPM systems.

Table 5.1: Performance of Optically Preamplified PDM-BPSK M-ary PPM Systems at a BER of 10^{-3}.

	PB-4-PPM	PB-8-PPM	PB-16-PPM	PB-32-PPM	PB-64-PPM
E_b/N_0 (dB)	5.3	4.75	4.3	3.95	3.65
PPB ($n_{sp} = 1$)	3.4	3	2.7	2.48	2.32
PPB ($n_{sp} = 3$)	10.2	9	8.1	7.44	6.96

Table 5.2: Performance of Optically Preamplified PDM-QPSK M-ary PPM Systems at a BER of 10^{-3}.

	PQ-4-PPM	PQ-8-PPM	PQ-16-PPM	PQ-32-PPM	PQ-64-PPM
E_b/N_0 (dB)	4.9	4.35	3.9	3.6	3.35
PPB ($n_{sp} = 1$)	3.1	2.7	2.45	2.29	2.16
PPB ($n_{sp} = 3$)	9.3	8.1	7.35	6.87	6.48

Table 5.3: Performance of Direct Detection Optically Preamplified M-ary PPM Systems with two ASE Noise sources at a BER of 10^{-3}.

	4-PPM	8-PPM	16-PPM	32-PPM	64-PPM
E_b/N_0 (dB)	9	7.6	6.7	6	5.5
PPB ($n_{sp} = 1$)	7.94	5.75	4.7	4	3.55
PPB ($n_{sp} = 3$)	15.88	17.26	14.1	12	10.65

(c) Finite Extinction Ratio Penalty for PDM-BPSK M-ary and PDM-QPSK M-ary PPM

The penalty due to finite ER was also evaluated. For PDM-QPSK 8-ary PPM systems, the penalty at 20 dB ER is 0.5 dB and for PDM-QPSK 16-ary PPM systems is 1.5

dB while for PDM-BPSK 8-ary and 16-ary PPM systems is 1 dB and 2.6 dB, respectively. For 64-ary PPM systems combined with PDM-QPSK or PDM-BPSK, the penalty at 20 dB ER is much larger than 7 dB, which indicates the impracticality of these systems.

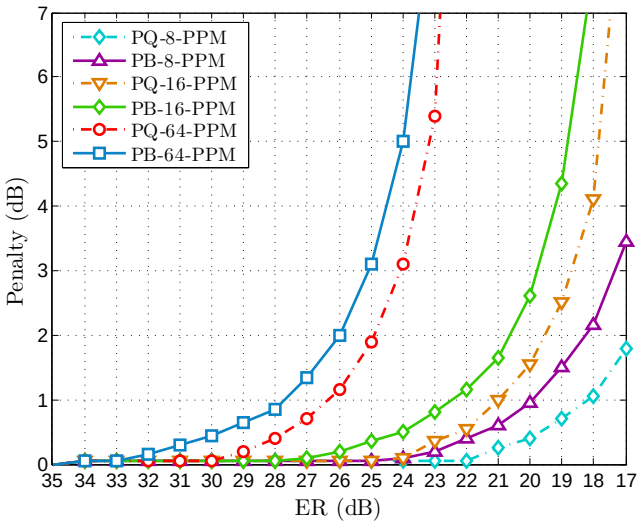

Figure 5.9: Performance Penalty Due to Finite ER.

Chapter 6

Conclusion and Future Work

This thesis provides the E_b/N_0 values required to obtain a BER of 10^{-3} for four optically preamplified systems. These systems are the direct detection OOK systems, the direct detection M-ary PPM systems, the coherent PDM-BPSK M-ary PPM systems, and the coherent PDM-QPSK M-ary PPM systems. The obtained E_b/N_0 values are to be used with proper FEC codes to reduce the achievable BER from 10^{-3} down to 10^{-12}.

The BER performance of optically preamplified direct detection 16-ary and 64-ary PPM systems is provided. Simulation techniques were used to evaluate the BER without assuming that the noise at the decision sample is Gaussian. The combined effects of the dual polarized amplifier noise, the Fabry-Pérot optical filter, the extinction ratio of the optical transmitter, and the electric filtering at the receiver are all considered in the evaluation. Extensive simulations were carried out to optimize the bandwidths of the optical and electrical filters at the receiver. Furthermore, the performance penalties due to frequency drift and timing jitter at the receiver are calculated. Simulation results provide the E_b/N_0 values at a target BER of 10^{-3} for four systems with different pulse shapes under an ER of 20 dB. In each case, the optimum filters were used. For 16-ary PPM systems, the E_b/N_0 values are 8 dB for the rectangular pulse shape and 8.2 dB for the $\sin^2$ pulse shape. For 64-ary PPM systems, the E_b/N_0 values are 8.35 dB and 9.6 dB for the rectangular pulse shape and the $\sin^2$ pulse shape, respectively. This result indicates that under an ER value of 20 dB, 16-ary PPM systems outperform 64-ary PPM systems.

The performance of optically preamplified coherent M-ary PPM combined with PDM-BPSK and with PDM-QPSK systems is also provided. For PDM-QPSK M-ary PPM systems, the E_b/N_0 values at a target BER of 10^{-3} for 8-ary, 16-ary and 64-ary PPM systems are 4.35 dB, 3.9 dB, and 3.6 dB, respectively. For PDM-BPSK M-ary PPM systems, the values are 4.75 dB, 4.3 dB, and 3.95 dB, respectively. The performance penalties due to finite ER values are also provided. For PDM-QPSK 8-ary PPM systems, the penalty at an ER value of 20 dB is 0.5 dB and for PDM-QPSK 16-ary PPM systems is 1.5 dB, while for PDM-BPSK 8-ary and 16-ary PPM systems is 1 dB and 2.6 dB, respectively. For 64-ary PPM systems combined with PDM-QPSK or PDM-BPSK, the penalty at 20 dB ER is much larger than 7 dB, which indicates the impracticality of these systems.

Future work will include the investigation of:

- The effects of employing other optical bandpass filters such as Bragg Grating and Gaussian filters in optically preamplified direct detection M-ary PPM receivers.
- Several hardware designs for the M-ary PPM receiver at high bit rate such as 10 Gbps.
- Practical issues related to the realization of optical phase lock loops (OPLL) for BPSK homodyne systems.
- The end-to-end performance of PDM-QPSK and PDM-BPSK M-ary PPM systems while taking into consideration the IQ imbalance effects.
- The performance degradation due to atmospheric effects on optically preamplified M-ary PPM systems and PDM-QPSK and PDM-BPSK M-ary PPM systems.
- The coding gain for different families of error correcting codes in the above systems.

References

[1] M. Toyoshima, W. R. Leeb, H. Kunimori, and T. Takano, "Comparison of microwave and light wave communication systems in space applications," pp. 59621U–59621U–12, 2005.

[2] S. Kartalopoulos, *Free Space Optical Networks for Ultra-Broad Band Services*. Wiley-IEEE Press, 2011.

[3] Z. Sodnik, B. Furch, and H. Lutz, "Optical intersatellite communication," *Selected Topics in Quantum Electronics, IEEE Journal of*, vol. 16, pp. 1051 –1057, sept.-oct. 2010.

[4] H. Hemmati, *Near-Earth Laser Communications*. CRC Press, 2009.

[5] S. Muhammad, T. Plank, E. Leitgeb, A. Friedl, K. Zettl, T. Javornik, and N. Schmitt, "Challenges in establishing free space optical communications between flying vehicles," in *Communication Systems, Networks and Digital Signal Processing, 2008. CNSDSP 2008. 6th International Symposium on*, pp. 82–86, 2008.

[6] E. Leitgeb, K. Zettl, S. Muhammad, N. Schmitt, and W. Rehm, "Investigation in free space optical communication links between unmanned aerial vehicles (UAVs)," in *Transparent Optical Networks, 2007. ICTON '07. 9th International Conference on*, vol. 3, pp. 152–155, 2007.

[7] Y. Koishi, Y. Suzuki, T. Takahashi, I. Mase, M. Jibiki, Y. Hashimoto, S. Murata, T. Yamashita, and K. Shiratama, "Research and development of 40 Gbps optical free space communication from satellite/airplane," in *Space Optical Systems and Applications (ICSOS), 2011 International Conference on*, pp. 88–92, 2011.

[8] F. Fidler, M. Knapek, J. Horwath, and W. Leeb, "Optical communications for high-altitude platforms," *Selected Topics in Quantum Electronics, IEEE Journal of*, vol. 16, pp. 1058 –1070, sept.-oct. 2010.

[9] E. Cianca, R. Prasad, M. De Sanctis, A. De Luise, M. Antonini, D. Teotino, and M. Ruggieri, "Integrated satellite-HAP systems," *Communications Magazine, IEEE*, vol. 43, no. 12, pp. supl.33–supl.39, 2005.

[10] N. Perlot, E. Duca, J. Horwath, D. Giggenbach, and E. Leitgeb, "System requirements for optical HAP-satellite links," in *Communication Systems, Networks and Digital Signal Processing, 2008. CNSDSP 2008. 6th International Symposium on*, pp. 72–76, 2008.

[11] F. Fidler, "Optical backhaul links between HAPs and satellites in the multi-gigabit regime," in *GLOBECOM Workshops, 2008 IEEE*, pp. 1–5, 2008.

[12] M. Antonini, S. BETTI, V. Carrozzo, E. Duca, and M. Ruggieri, "Feasibility analysis of a HAP-LEO optical link for data relay purposes," in *Aerospace Conference, 2006 IEEE*, pp. 7 pp.–, 2006.

[13] R. Fields, D. Kozlowski, H. Yura, R. Wong, J. Wicker, C. Lunde, M. Gregory, B. Wandernoth, and F. Heine, "5.625 Gbps bidirectional laser communications measurements between the nfire satellite and an optical ground station," in *Space Optical Systems and Applications (ICSOS), 2011 International Conference on*, pp. 44–53, 2011.

[14] R. Daddato, K.-J. Schulz, and I. Zayer, "Deep space science downlinks via optical communication," in *Space Optical Systems and Applications (ICSOS), 2011 International Conference on*, pp. 8–13, 2011.

[15] B. Moision, J. Wu, and S. Shambayati, "An optical communications link design tool for long-term mission planning for deep-space missions," in *Aerospace Conference, 2012 IEEE*, pp. 1–12, 2012.

[16] D. O. Caplan, "Laser communication transmitter and receiver design," *Journal of Optical and Fiber Communications Research*, vol. 4, pp. 225–362, 2007. 10.1007/s10297-006-0079-z.

[17] P. Winzer, M. Pfennigbauer, M. Strasser, and W. Leeb, "Optimum filter bandwidths for optically preamplified NRZ receivers," *Lightwave Technology, Journal of*, vol. 19, pp. 1263 –1273, sep 2001.

[18] A. Waseda, M. Sasaki, M. Takeoka, M. Fujiwara, M. Toyoshima, and A. Assalini, "Numerical evaluation of coherent signals for deep-space links," in *Space Optical Systems and Applications (ICSOS), 2011 International Conference on*, pp. 334–342, 2011.

[19] M. Knapek, J. Horwath, F. Moll, B. Epple, N. Courville, H. Bischl, and D. Giggenbach, "Optical high-capacity satellite downlinks via high-altitude platform relays," pp. 67090E–67090E–12, 2007.

[20] R. Cryan and R. Unwin, "Optical space communications employing pulse position modulation," in *Advanced Modulation and Coding Techniques for Satellite Communications, IEE Colloquium on*, pp. 7/1–7/5, 1992.

[21] D. Caplan, B. Robinson, M. Stevens, D. Boroson, and S. Hamilton, "High-rate photon-efficient laser communications with near single photon/bit receiver sensitivities," in *Optical Fiber Communication Conference, 2006 and the 2006 National Fiber Optic Engineers Conference. NFOEC 2006*, p. 3 pp., march 2006.

[22] F. Xu, M. Khalighi, and S. Bourennane, "Pulse position modulation for FSO systems: Capacity and channel coding," in *Telecommunications, 2009. ConTEL 2009. 10th International Conference on*, pp. 31 –38, june 2009.

[23] A. Waseda, M. Sasaki, M. Takeoka, M. Fujiwara, M. Toyoshima, and A. Assalini, "Numerical evaluation of PPM for deep-space links," *Optical Communications and Networking, IEEE/OSA Journal of*, vol. 3, no. 6, pp. 514–521, 2011.

[24] X. Liu, T. Wood, R. Tkach, and S. Chandrasekhar, "Demonstration of record sensitivities in optically preamplified receivers by combining PDM-QPSK and M-ary pulse-position modulation," *Lightwave Technology, Journal of*, vol. 30, pp. 406 –413, feb.15, 2012.

[25] D. Begley, "Free-space laser communications: a historical perspective," in *Lasers and Electro-Optics Society, 2002. LEOS 2002. The 15th Annual Meeting of the IEEE*, vol. 2, pp. 391–392 vol.2, 2002.

[26] G. D. Fletcher, T. R. Hicks, and B. Laurent, "The SILEX optical interorbit link experiment," *Electronics Communication Engineering Journal*, vol. 3, no. 6, pp. 273–279, 1991.

[27] S. Yamakawa, T. Hanada, and H. Kohata, "R&D status of the next generation optical communication terminals in JAXA," in *Space Optical Systems and Applications (ICSOS), 2011 International Conference on*, pp. 389–393, 2011.

[28] H. Hemmati, *Deep Space Optical Communications*. Wiley Interscience, 2009.

[29] G. H. S. R. Ramaswami, K. N. Sivarajan, *Optical Networks: A Practical Prespective*. Morgan Kaufmann, 2010.

[30] H. Keang-Po, *Phase-Modulated Optical Communication Systems*. Springer, 2005.

[31] S. Chinn, D. Boroson, and J. Livas, "Sensitivity of optically preamplified DPSK receivers with fabry pérot filters," *Lightwave Technology, Journal of*, vol. 14, pp. 370 –376, mar 1996.

[32] D. Caplan, M. Stevens, J. Carney, and R. Murphy, "Demonstration of optical DPSK communication with 25 photons/bit receiver sensitivity," in *Lasers and Electro-Optics, 2006 and 2006 Quantum Electronics and Laser Science Conference. CLEO/QELS 2006. Conference on*, pp. 1–2, 2006.

[33] S. Benedetto, R. Gaudino, and P. Poggiolini, "Direct detection of optical digital transmission based on polarization shift keying modulation," *Selected Areas in Communications, IEEE Journal on*, vol. 13, no. 3, pp. 531–542, 1995.

[34] F. Fidler, J. Grosinger, and W. Leeb, "Sensitivity of balanced receivers for polarization shift keying in free-space optical communications," in *Optical Communication, 2009. ECOC '09. 35th European Conference on*, pp. 1–2, 2009.

[35] S. Benedetto, R. Gaudino, and P. Poggiolini, "Performance of coherent optical polarization shift keying modulation in the presence of phase noise," *Communications, IEEE Transactions on*, vol. 43, no. 234, pp. 1603–1612, 1995.

[36] C. Liu, Y. Sun, Y. Yao, and X. Zhao, "Analysis of direct detection and coherent detection in wireless optical communication with polarization shift keying," in *Lasers Electro Optics The Pacific Rim Conference on Lasers and Electro-Optics, 2009. CLEO/PACIFIC RIM '09. Conference on*, pp. 1–2, 2009.

[37] A. Fletcher, T. Royster, N. List, and R. Shoup, "Optical M-PPM signaling with binary forward error correction," in *Military Communications Conference, 2010 - MILCOM 2010*, pp. 779 –784, 31 2010-nov. 3 2010.

[38] A. Phillips, R. Cryan, and J. Senior, "Novel laser intersatellite communication system employing optically preamplified PPM receivers," *Communications, IEE Proceedings-*, vol. 142, pp. 15 –20, feb 1995.

[39] N. Spellmeyer, S. Bernstein, D. Boroson, D. Caplan, A. Fletcher, S. Hamilton, R. Murphy, M. Norvig, H. Rao, B. Robinson, S. Savage, R. Schulein, M. Stevens, and J. Wang, "Demonstration of multi-rate thresholded preamplified 16-ary pulse-position-modulation," in *Optical Fiber Communication (OFC), collocated National Fiber Optic Engineers Conference, 2010 Conference on (OFC/NFOEC)*, pp. 1 –3, march 2010.

[40] D. Caplan, B. Robinson, R. Murphy, and M. Stevens, "Demonstration of 2.5-Gslot/s optically-preamplified M-PPM with 4 photons/bit receiver sensitivity," in *Optical Fiber Communication Conference, 2005. Technical Digest. OFC/NFOEC*, vol. 6, pp. 3 pp. Vol. 5–, 2005.

[41] A. Mendez, R. Gagliardi, V. Hernandez, and C. Bennett, "Receiver architecture for 12.5 GB/S 16-ary pulse position modulation (PPM) signaling," in *Avionics, Fiber-Optics and Photonics Technology Conference, 2008 IEEE*, pp. 59 –60, 30 2008-oct. 2 2008.

[42] A. Phillips, R. Cryan, and J. Senior, "Performance evaluation of optically preamplified PPM systems," *Photonics Technology Letters, IEEE*, vol. 6, pp. 651 –653, may 1994.

[43] A. Phillips, R. Cryan, and J. Senior, "Optically preamplified pulse-position modulation for fibre-optic communication systems," *Optoelectronics, IEE Proceedings -*, vol. 143, no. 2, pp. 153–159, 1996.

[44] P. Theodorou and J. M. H. Elmirghani, "Selective multi-channel coherent optically preamplified systems: sensitivity assessment," in *Global Telecommunications Conference, 1997. GLOBECOM '97., IEEE*, vol. 1, pp. 275–279 vol.1, 1997.

[45] D. J. Geisler, T. M. Yarnall, W. E. Keicher, M. L. Stevens, A. M. Fletcher, R. R. Parenti, D. O. Caplan, and S. A. Hamilton, "Demonstration of 2.1 photon-per-bit sensitivity for BPSK at 9.94-Gb/s with rate-$\frac{1}{2}$ FEC," in *Optical Fiber Communication Conference/National Fiber Optic Engineers Conference 2013*, p. OM2C.6, Optical Society of America, 2013.

[46] E. Ip, D. Buchter, C. Langrock, J. Kahn, H. Herrmann, W. Sohler, and M. Fejer, "QPSK transmission over free-space link at 3.8 μm using coherent detection with wavelength conversion," in *Optical Communication, 2008. ECOC 2008. 34th European Conference on*, pp. 1–2, 2008.

[47] B. Patnaik and P. K. Sahu, "Novel QPSK modulation technique for DWDM free space optical communication system," in *Wireless and Optical Communications Conference (WOCC), 2012 21st Annual*, pp. 140–145, 2012.

[48] T. Pfau, R. Peveling, V. Herath, S. Hoffmann, C. Wordehoff, O. Adamczyk, M. Porrmann, and R. Noe, "Towards real-time implementation of coherent optical communication," in *Optical Fiber Communication - incudes post deadline papers, 2009. OFC 2009. Conference on*, pp. 1–3, 2009.

[49] E. Dutisseuil, J.-M. Tanguy, A. Voicila, R. Laube, F. Bore, H. Takeugming, F. de Dinechin, F. Cerou, and G. Charlet, "34 Gb/s PDM-QPSK coherent receiver using SiGe ADCs and a single FPGA for digital signal processing," in *Optical Fiber Communication Conference and Exposition (OFC/NFOEC), 2012 and the National Fiber Optic Engineers Conference*, pp. 1–3, 2012.

[50] A. Pinto and F. Guiomar, "Flexible optical receivers," in *Transparent Optical Networks (ICTON), 2012 14th International Conference on*, pp. 1–4, 2012.

[51] M. Toyoshima, T. Sasaki, H. Takenaka, Y. Shoji, Y. Takayama, Y. Koyama, H. Kunimori, M. Akioka, M. Fujiwara, and M. Sasaki, "Research and development of free-space laser communications and quantum key distribution technologies at nict," in *Space Optical Systems and Applications (ICSOS), 2011 International Conference on*, pp. 1–7, 2011.

[52] T. Sasaki, M. Toyoshima, and H. Takenaka, "Digital coherent optical receiver for satellite laser communication," in *Space Optical Systems and Applications (ICSOS), 2011 International Conference on*, pp. 245–247, 2011.

[53] M. Karlsson and E. Agrell, "Which is the most power-efficient modulation format in optical links?," *Opt. Express*, vol. 17, pp. 10814–10819, Jun 2009.

[54] S. Chandrasekhar, X. Liu, T. Wood, and R. Tkach, "High sensitivity modulation formats," in *Optical Fiber Communication Conference and Exposition (OFC/NFOEC), 2012 and the National Fiber Optic Engineers Conference*, pp. 1–3, 2012.

[55] M. Karlsson and E. Agrell, "Generalized pulse-position modulation for optical power-efficient communication," in *Optical Communication (ECOC), 2011 37th European Conference and Exhibition on*, pp. 1–3, 2011.

[56] T. H. Wood, "Advanced modulation formats for free space laser communications," in *Optical Fiber Communication Conference/National Fiber Optic Engineers Conference 2013*, p. NM3F.5, Optical Society of America, 2013.

[57] X. Liu, S. Chandrasekhar, T. H. Wood, R. W. Tkach, P. J. Winzer, E. C. Burrows, and A. R. Chraplyvy, "M-ary pulse-position modulation and frequency-shift keying with additional polarization/phase modulation for high-sensitivity optical transmission," *Opt. Express*, vol. 19, pp. B868–B881, Dec 2011.

[58] X. Liu, T. Wood, R. Tkach, and S. Chandrasekhar, "Demonstration of record sensitivity in an optically pre-amplified receiver by combining PDM-QPSK and 16-PPM with pilot-assisted digital coherent detection," in *Optical Fiber Communication Conference and Exposition (OFC/NFOEC), 2011 and the National Fiber Optic Engineers Conference*, pp. 1–3, 2011.

[59] X. Liu, S. Chandrasekhar, T. Wood, R. Tkach, E. Burrows, and P. Winzer, "Demonstration of 2.7-PPB receiver sensitivity using PDM-QPSK with 4-PPM and unrepeatered transmission over a single 370-km unamplified ultra-large-area fiber span," in *Optical Communication (ECOC), 2011 37th European Conference and Exhibition on*, pp. 1–3, 2011.

[60] V. Chan, "Free-space optical communications," *Lightwave Technology, Journal of*, vol. 24, no. 12, pp. 4750–4762, 2006.

[61] S. K. Robert M. Gagliardi, *Optical Communications*. Wiley, 1995.

[62] G. Agrawal, *Fiber-Optic Communication Systems*. Wiley Interscience, 2002.

[63] S. Guha, J. Habif, and M. Takeoka, "PPM demodulation: On approaching fundamental limits of optical communications," in *Information Theory Proceedings (ISIT), 2010 IEEE International Symposium on*, pp. 2038–2042, 2010.

[64] S. Dolinar, B. Erkmen, B. Moision, K. Birnbaum, and D. Divsalar, "The ultimate limits of optical communication efficiency with photon-counting receivers," in *Information Theory Proceedings (ISIT), 2012 IEEE International Symposium on*, pp. 541–545, 2012.

[65] B. Robinson, D. Boroson, D. Burianek, and D. Murphy, "The lunar laser communications demonstration," in *Space Optical Systems and Applications (ICSOS), 2011 International Conference on*, pp. 54–57, 2011.

[66] N. Olsson, "Lightwave systems with optical amplifiers," *Lightwave Technology, Journal of*, vol. 7, no. 7, pp. 1071–1082, 1989.

[67] A. Papoulis, *Probability, Random Variables, and Stochastic Processes*. 3rd ed., 1991.

[68] S. Kartalopoulos, *Optical Bit Error Rate: An Estimation Methodology*. Wiley- IEEE Press, 2004.

[69] I. P. Kaminow, T. Li, and A. E. Willner, *Optical Fiber Telecommunications V B : Systems and Networks*. Academic Press, 2008.

[70] O. Tonguz and R. Wagner, "Equivalence between preamplified direct detection and heterodyne receivers," *Photonics Technology Letters, IEEE*, vol. 3, no. 9, pp. 835–837, 1991.

[71] J. G. Proakis and M. Salehi, *Digital Communications*. McGraw-Hill, 2008.

[72] B. P. Lathi, *Modern Digital and Analog Communication Systems*. Oxford University Press, 1998.

[73] P. A. Humblet and M. Azizoglu, "On the bit error rate of lightwave systems with optical amplifiers," *Lightwave Technology, Journal of*, vol. 11, pp. 1576–1582, sep 1991.

[74] L. Kazovsky and O. Tonguz, "Sensitivity of direct-detection lightwave receivers using optical preamplifiers," *Photonics Technology Letters, IEEE*, vol. 3, pp. 53 –55, jan. 1991.

[75] I. Monroy and G. Einarsson, "Bit error evaluation of optically preamplified direct detection receivers with fabry-perot optical filters," *Lightwave Technology, Journal of*, vol. 15, no. 8, pp. 1546–1553, 1997.

[76] M. Pfennigbauer, M. Strasser, M. Pauer, and P. Winzer, "Dependence of optically preamplified receiver sensitivity on optical and electrical filter bandwidths-measurement and simulation," *Photonics Technology Letters, IEEE*, vol. 14, no. 6, pp. 831–833, 2002.

[77] J. Rebola and A. V. T. Cartaxo, "New gaussian approximation for performance assessment of optically preamplified receivers with arbitrary optical and electrical filters," in *Lasers and Electro-Optics, 2001. CLEO/Pacific Rim 2001. The 4th Pacific Rim Conference on*, vol. 2, pp. II–316–II–317 vol.2, 2001.

[78] E. Forestieri and M. Secondini, "On the error probability evaluation in lightwave systems with optical amplification," *Lightwave Technology, Journal of*, vol. 27, no. 6, pp. 706–717, 2009.

[79] A. Tychopoulos, O. Koufopaulou, and I. Tomkos, "FEC in optical communications - a tutorial overview on the evolution of architectures and the future prospects of outband and inband FEC for optical communications," *Circuits and Devices Magazine, IEEE*, vol. 22, pp. 79 –86, nov.-dec. 2006.

[80] A. Elrefaie, J. Townsend, M. Romeiser, and K. Shanmugan, "Computer simulation of digital lightwave links," *Selected Areas in Communications, IEEE Journal on*, vol. 6, no. 1, pp. 94–105, 1988.

[81] A. Elrefaie, R. Wagner, D. Atlas, and D. Daut, "Chromatic dispersion limitations in coherent lightwave transmission systems," *Lightwave Technology, Journal of*, vol. 6, no. 5, pp. 704–709, 1988.

Vita

Sanaa Hamid was born in 1987 in the Kingdom of Saudi Arabia where she acquired her elementary and secondary education. In 2004, she was ranked ninth in the national Saudi secondary exams and later, she enrolled in the Electrical and Electronic Engineering Department in the University of Khartoum (UofK). In 2009, she graduated with the degree of Bachelor of Science (Honours) in Electrical and Electronic Engineering. After graduation, she worked as research assistant in the Electronic Systems Research Center (ESRC) in Khartoum and as a part-time teaching assistant in both UofK and Sudan University of Science and Technology. In 2011, she was awarded the graduate teaching assistantship from the American University of Sharjah (AUS) and joined the Electrical Engineering Master's program. During her Master's, she got two conference papers accepted and presented in two different IEEE conferences held at AUS: ICCSII'12 and ICCSPA'13. She has been an IEEE member since 2008 and a member of the Communication, Signal Processing and Photonics societies. Her research areas of interest are optical and wireless communications, digital signal processing, computer networking, queuing theory and systems modeling.